IV Geant4 International User Conference at the physics-medicine-biology frontier

Napoli, October 24th-26th, 2022

Monte Carlo for Nuclear Medicine: vision and future requirements

Prof. Ernesto Amato

University of Messina

Department of Biomedical Sciences and of Morphologic and Functional Imaging

University Hospital “Gaetano Martino” - Messina

National Italian Institute of Nuclear Physics (INFN)

Section of Catania

Monte Carlo for Nuclear Medicine: vision and future requirements CONCLUSIONS

- Vision? *Only a personal perspective...*
- Future requirements?
  - Powerful HW? *Already here*
  - Accurate MC tools & user-friendly interfaces?

    Already present, but:
    - Need for accurate validation of new versions
    - Crucial the completeness of source terms (radioactive decays)
    - Clarity of documentation of MC codes and interfaces
  - Direct involvement (or *at least* close collaboration) in hospitals as medical physicists and radiation protection experts, to identify together with clinicians the <u>really USEFUL studies and applications</u>

Applications of MC in NM

- Internal dosimetry
  - Organ-level dosimetry: S factors
  - 3D dosimetry: VSVs and DPKs
  - Direct MC dosimetry
- Small-scale dosimetry and microdosimetry
  - Tissutal structure
  - Cellular and multi-cellular models
- Radioprotection: optimization of shielding
- Production of radionuclides: optimization of reactions and targetry
- Design of novel scanners

Shielding applications

- Shielding of beta sources with plastics (and secondary high-Z absorbers)
- Evaluation of skin dose and dose to the extremities during handling of sources and in cases of contamination

Beta shielding

The shielding of beta sources during manipulation is obtained with low-Z materials, which are able to absorb the high energy electrons maximizing their energy loss by inelasting collisions and thus minimizing the energy losses by radiative (bremsstrahlung) X-ray emission.
The small amount of bremsstrahlung emission can be attenuated by an outer high-Z shield.

Requirements:

- Transparency
- Thermal conductivity
- Elasticity
- Operating range of temperatures

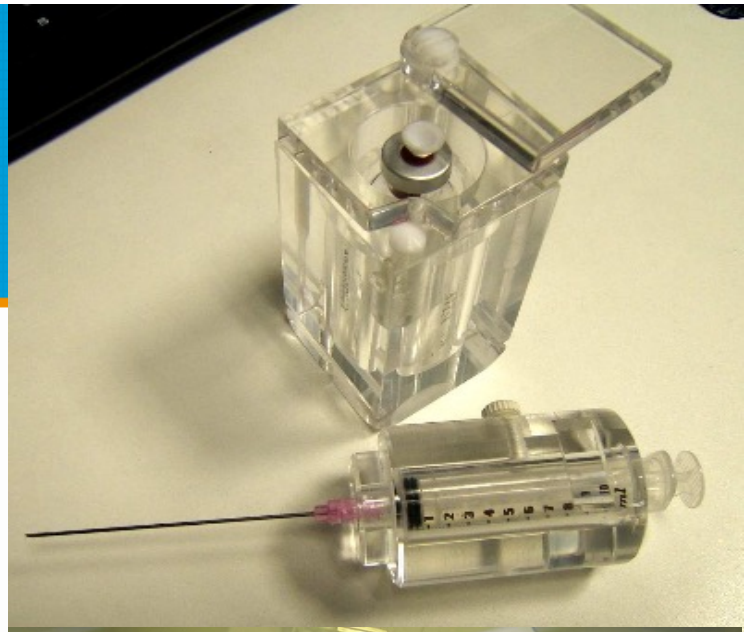

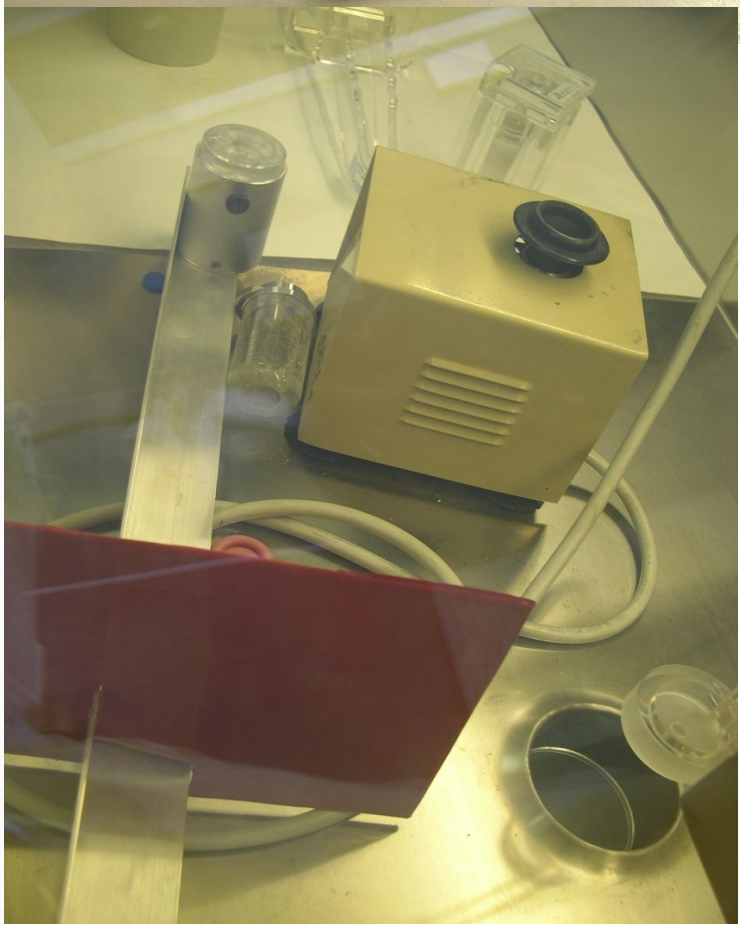

Shielding of ^{90}Y betas in plastics

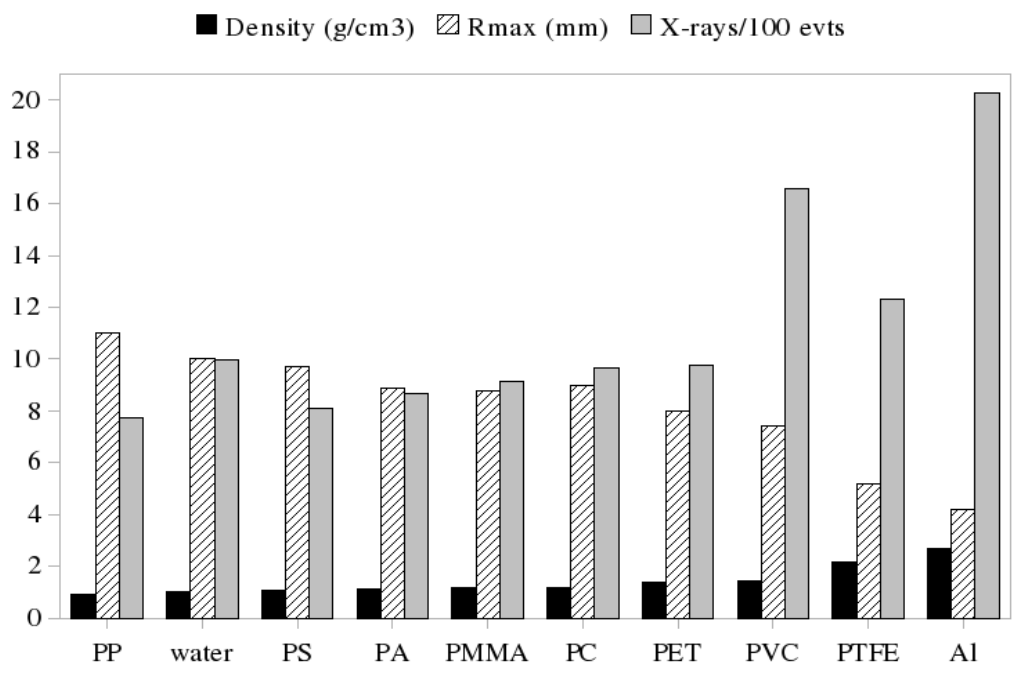

Max. beta ranges and fluence of X-rays

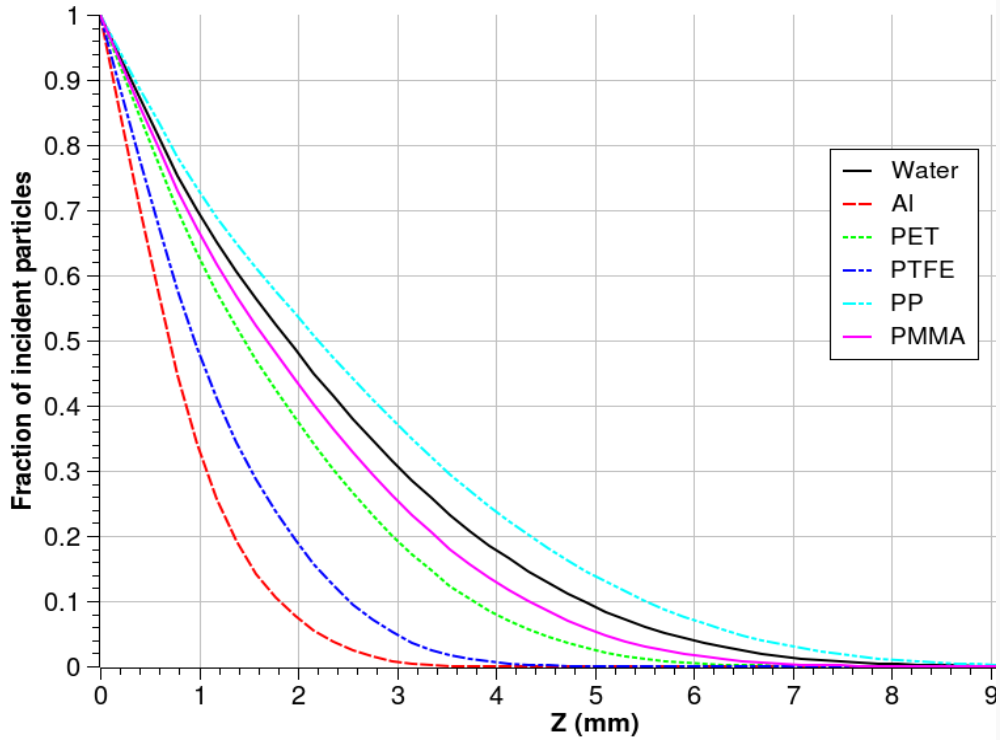

Absorption curves in materials

E. Amato and D. Lizio. "Plastic materials as a radiation shield for β^- sources: a comparative study through Monte Carlo calculation." Journal of Radiological Protection 29 (2009) 239.

^{90}Y source in glass vial with PTFE shield

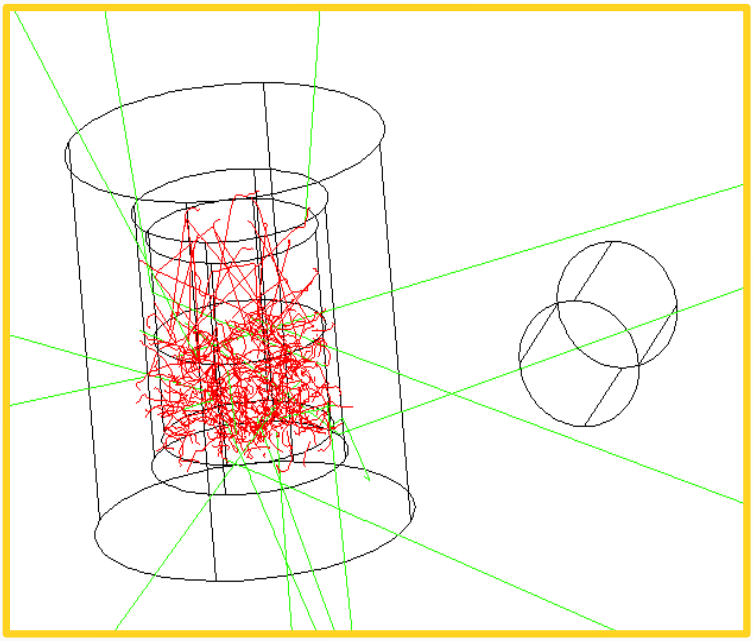

Opaque, but
high-temperature resistant

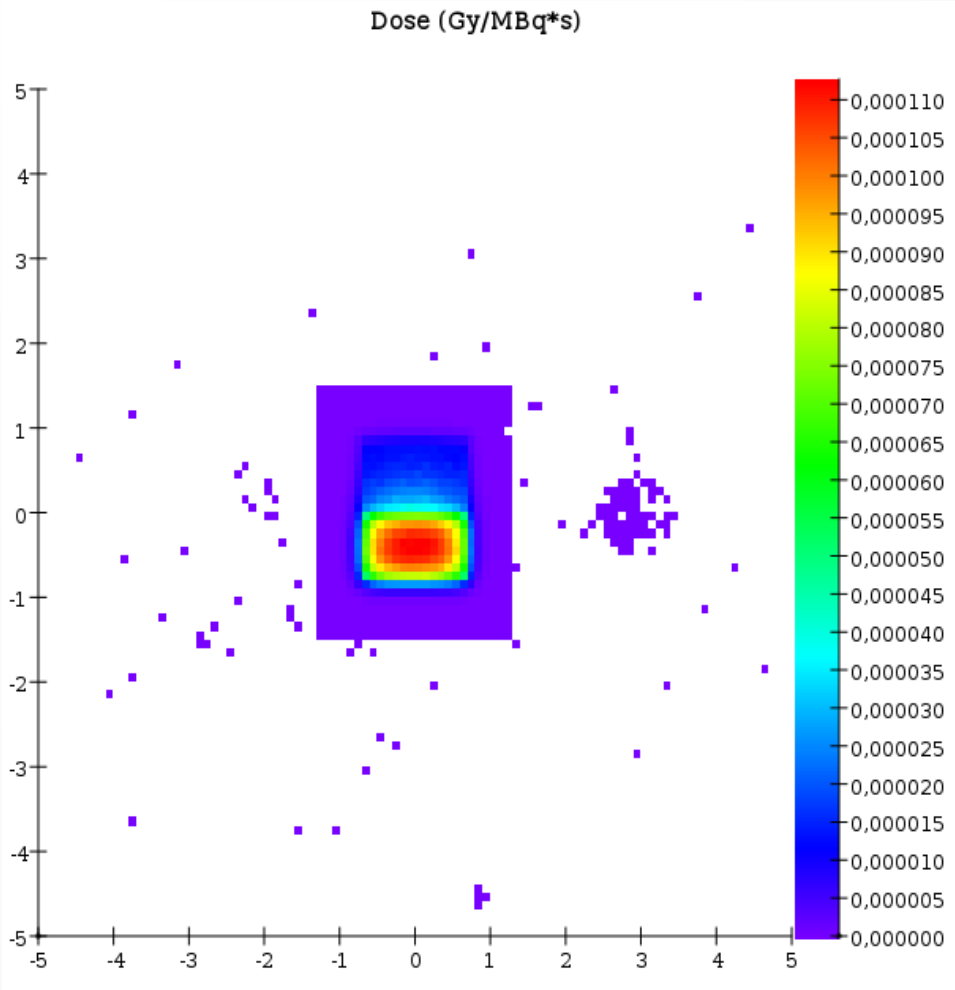

Dimensions (mm):

- vial: D=16 H=20 thick=1
- water source: half vial
- PTFE shield thick= 5
- “finger”: D=10 V=1 cm^3 at 30 from the source centre.

^{90}Y source in glass vial with PMMA shield

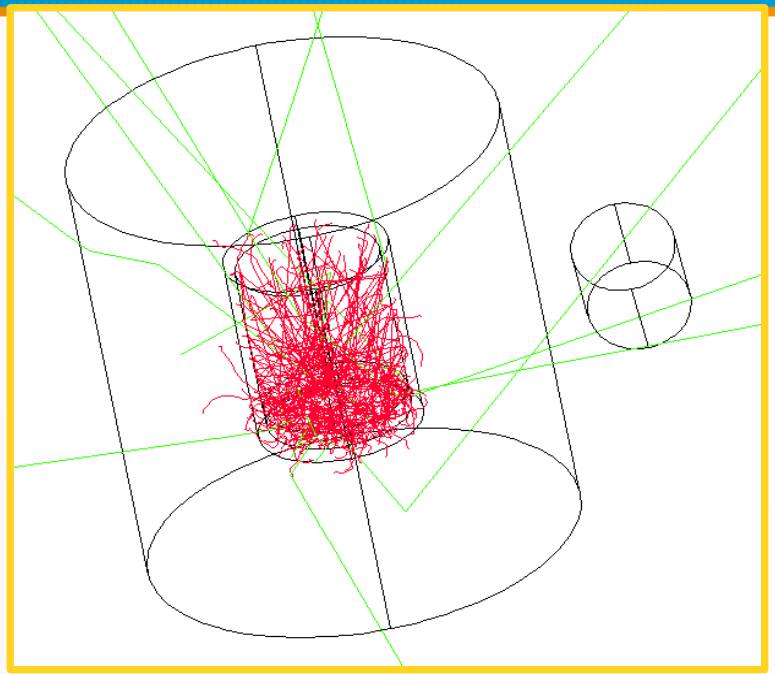

Transparent

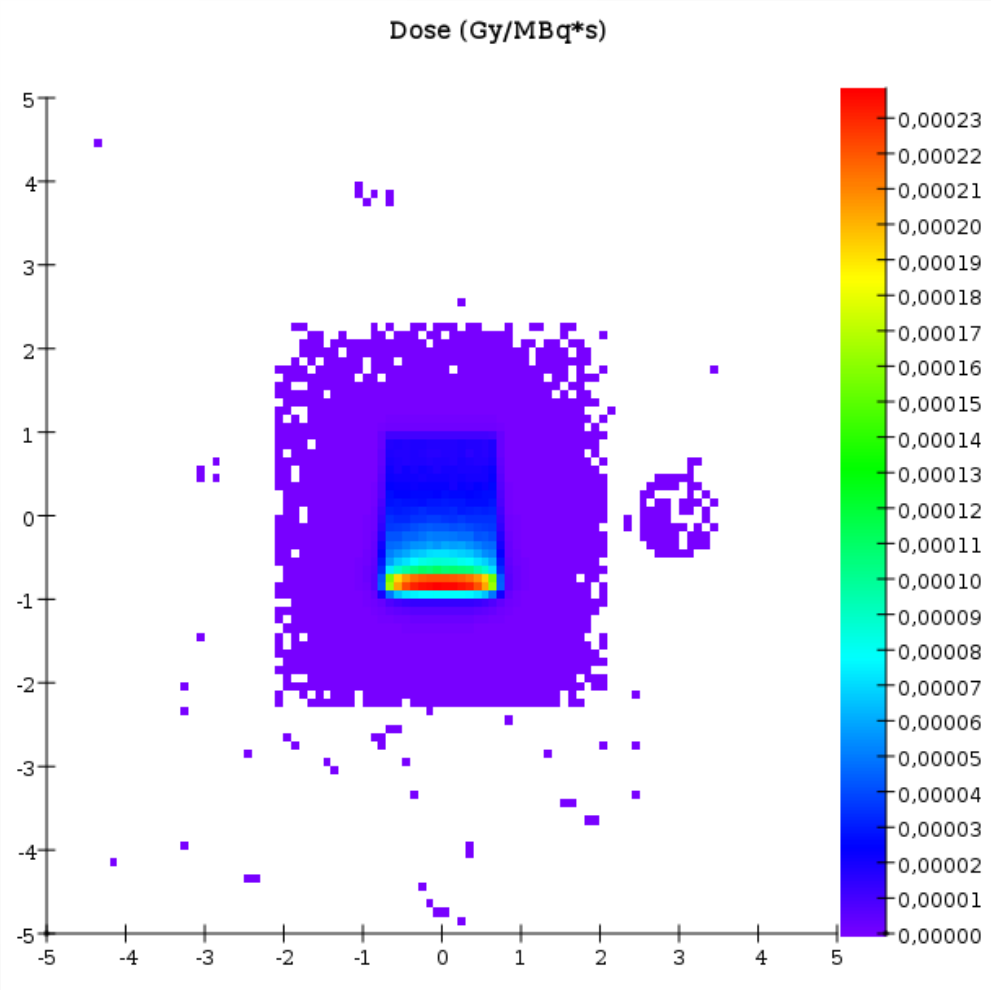

Dimensions (mm):

- vial: D=16 H=20 thick=1
- water source: H=2
- PMMA shield thick=13
- "finger": D=10 V=1 cm^3 at 35 from the source centre.

^{177}Lu source in glass vial with PMMA and W shields

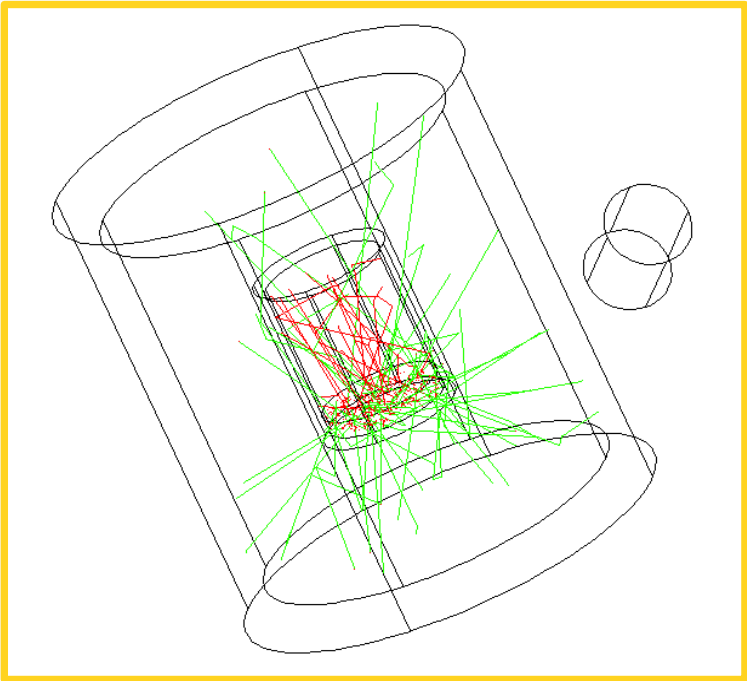

Dimensions (mm):

- vial: D=16 H=20 thick=1
- water source: H=2
- PMMA shield thick=13
- W shield thick=4
- “finger”: D=10 V=1 cm^3 at 35 from the source centre.

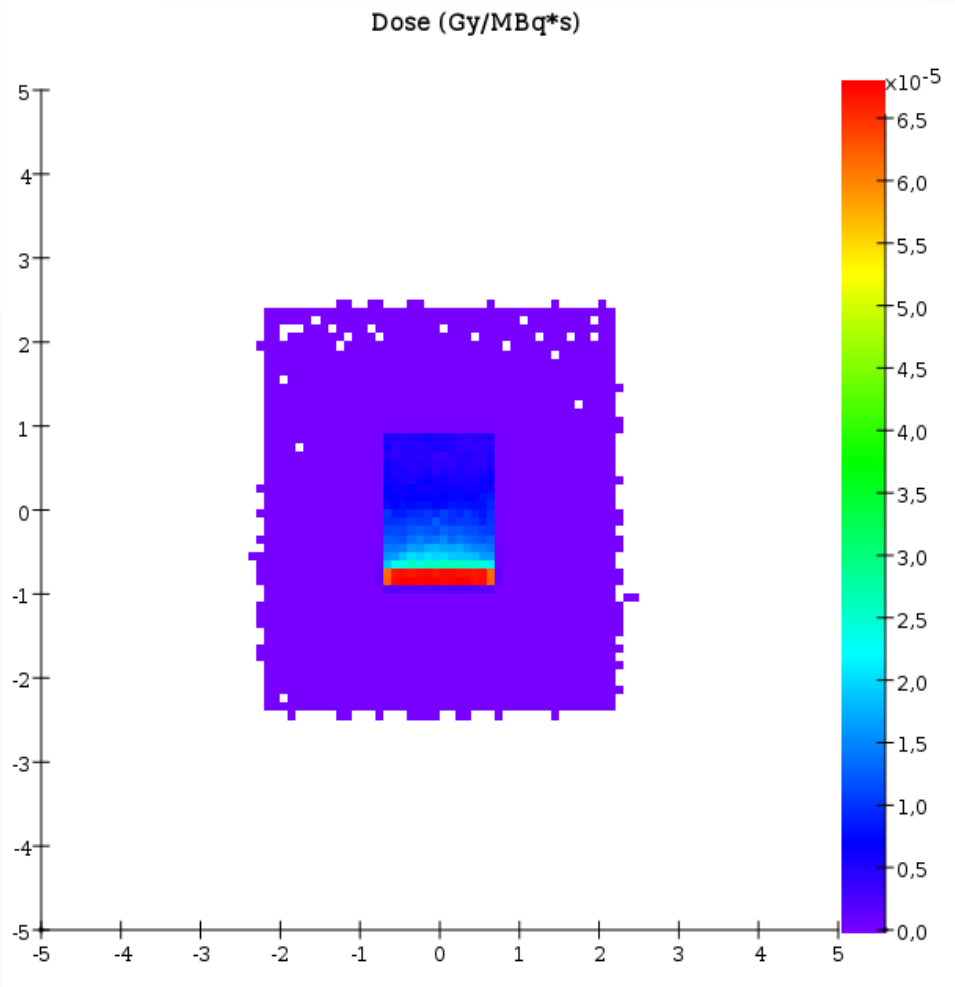

Skin dose evaluation

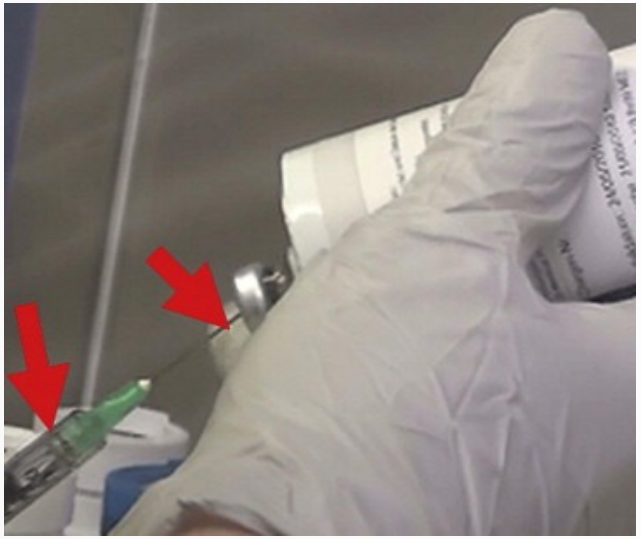

Manipulation of shielded vials

Contamination of the skin

Contamination of tables and surfaces

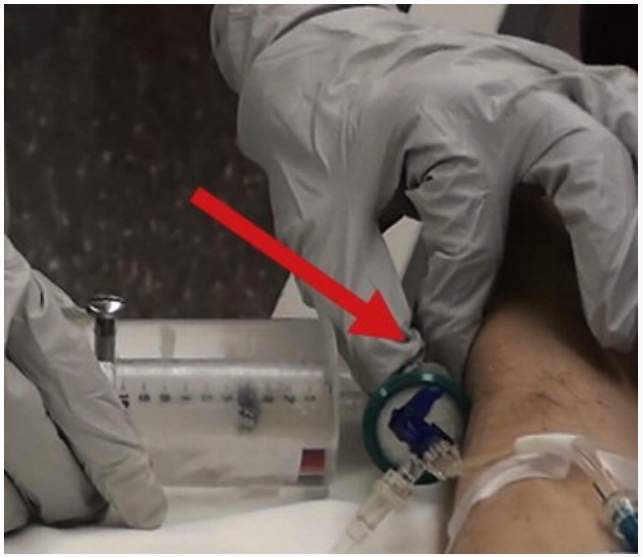

VARSKIN code

(RAMP - NRC)

RAMP Website
Radiation Protection Computer Code Analysis and Maintenance Program

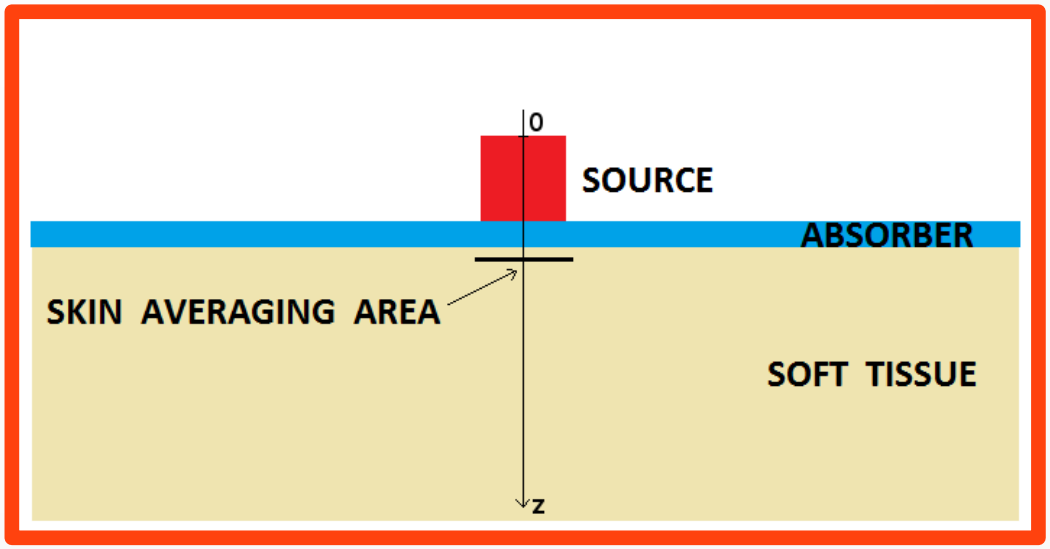

Comparison Varskin vs. MC Gamos

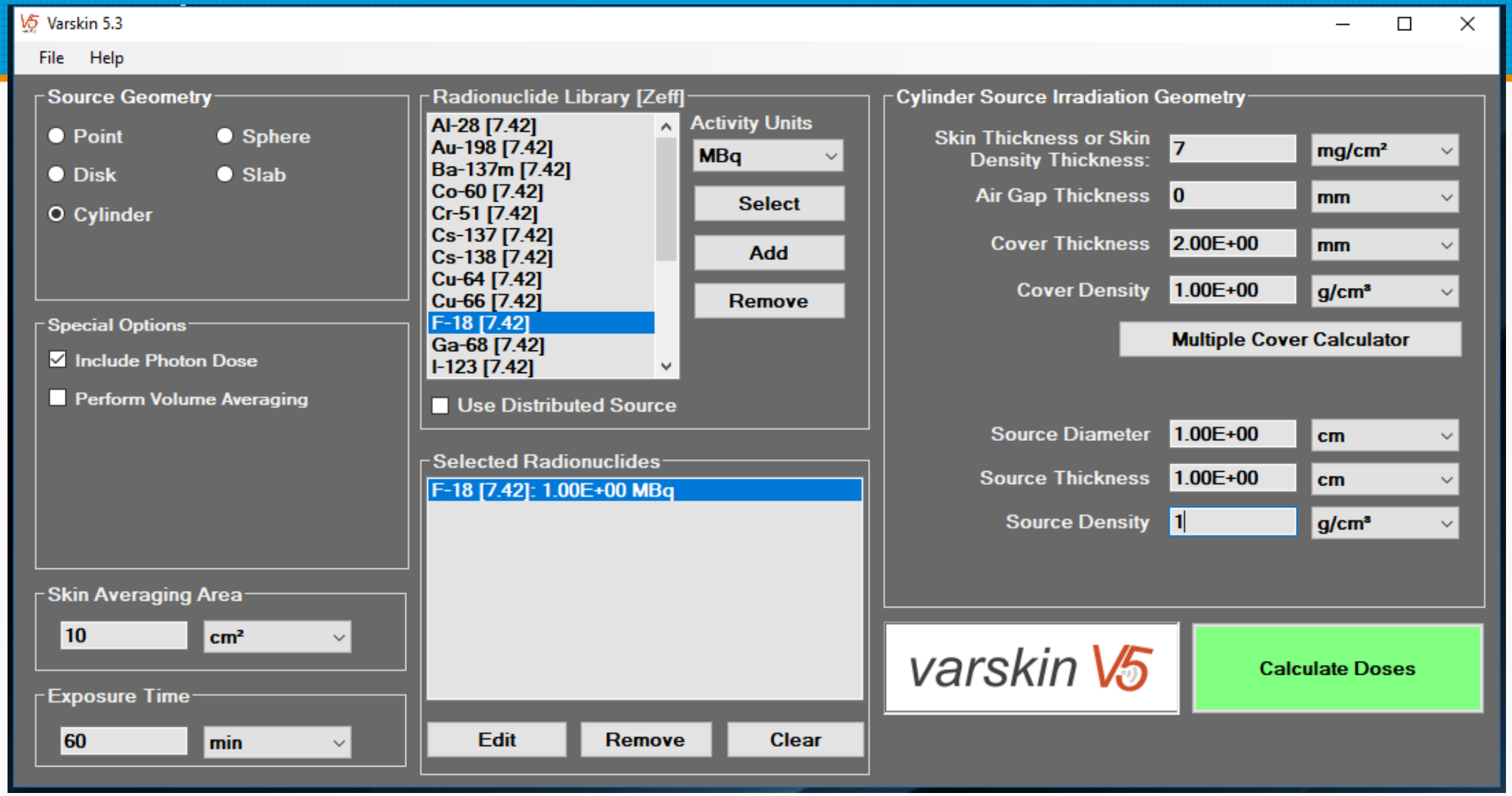

E. Amato and A. Italiano. "Evaluation of skin absorbed doses during manipulation of radioactive sources: a comparison between the VARSKIN code and Monte Carlo simulations." Journal of Radiological Protection 38 (2018): 262.

Comparison Varskin vs. MC Gamos

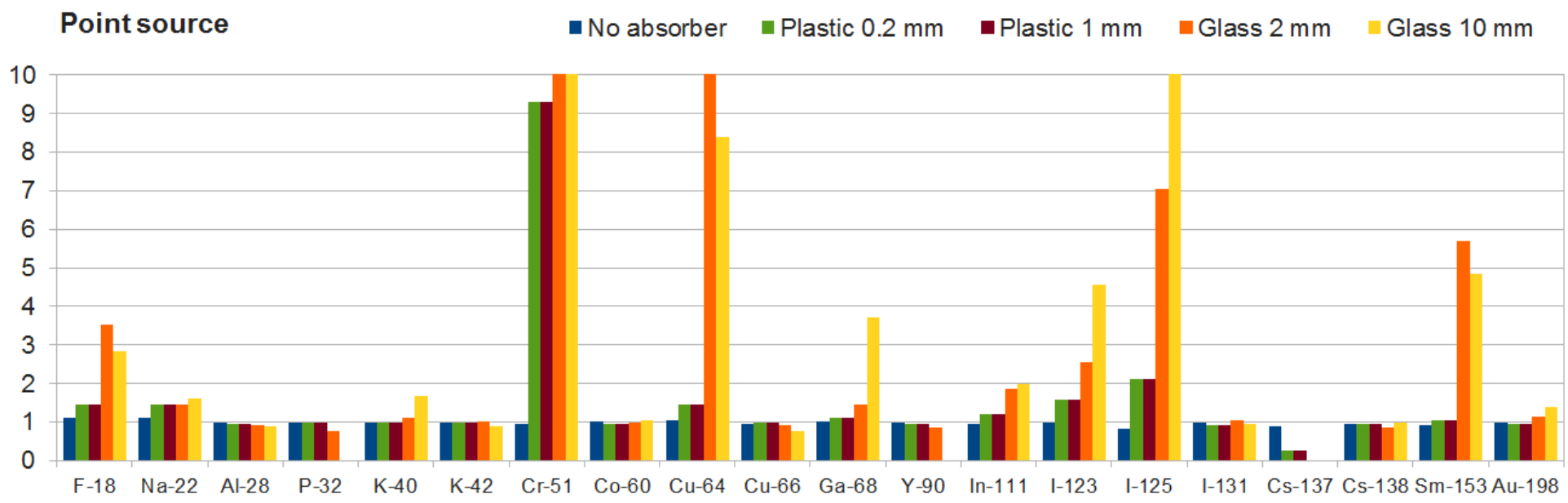

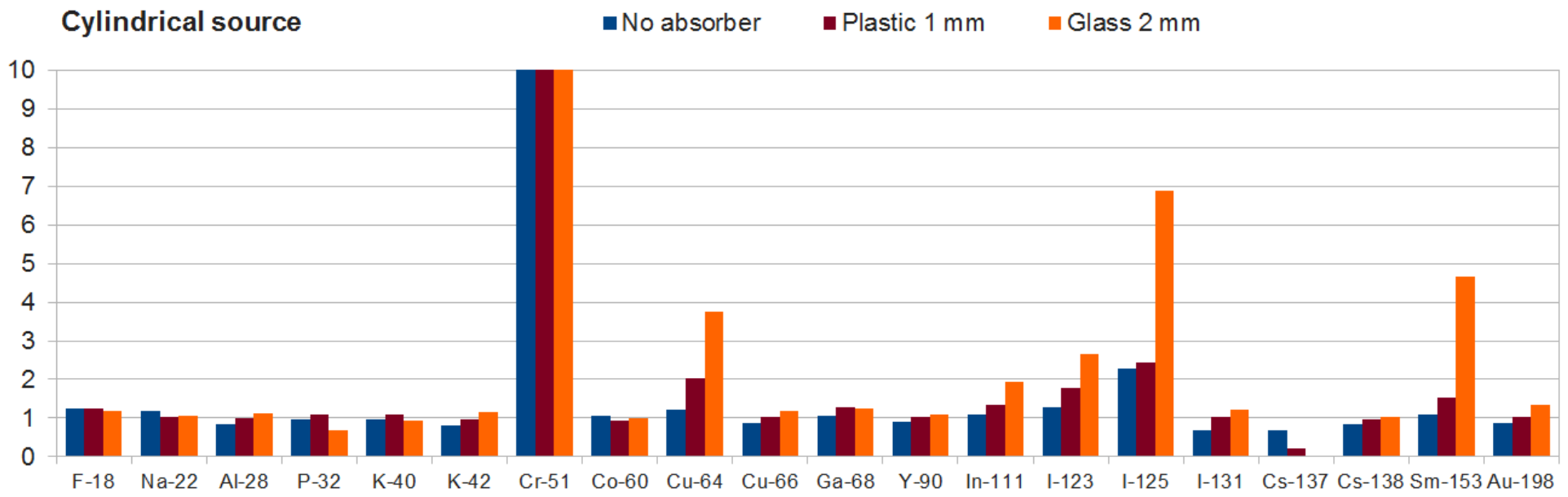

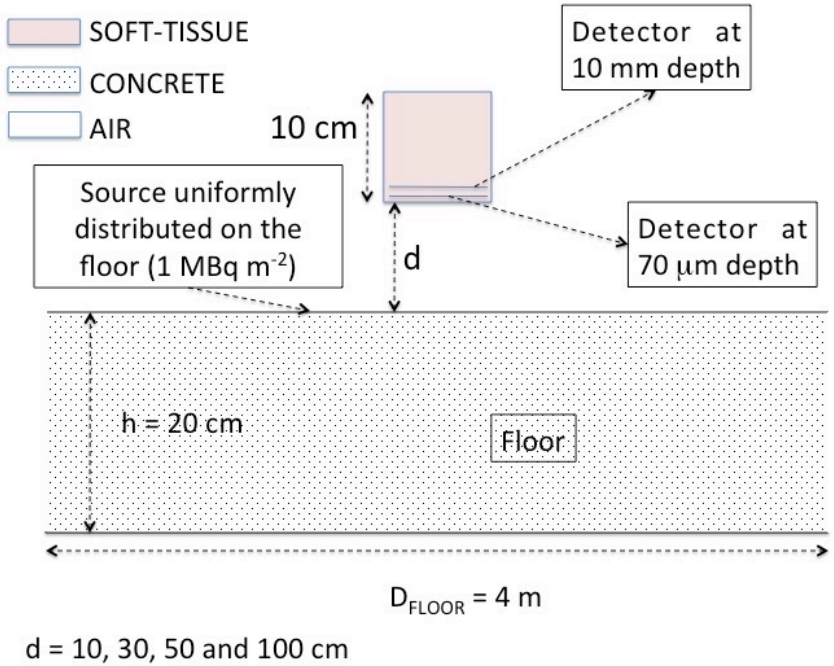

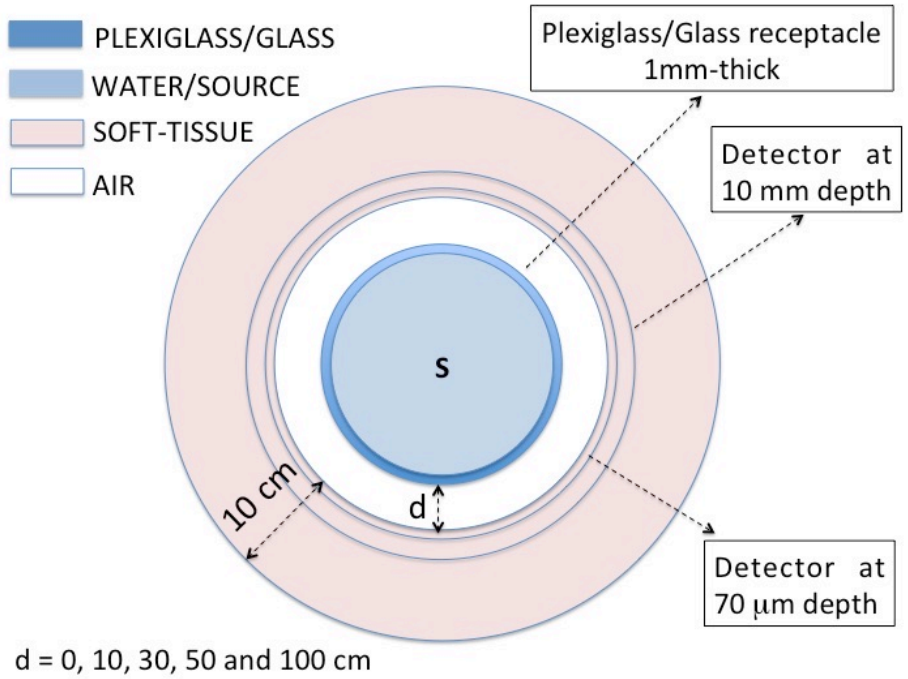

Table 8 Skin and deep doses evaluated as a function of the distance for a plexiglass receptacle (2-cm diameter) filled with 20 ml of radioactive solution.

	D (mSv/MBqh)									
	d = 0 cm		d = 10 cm		d = 30 cm		d = 50 cm		d = 100 cm	
	Skin	Deep	Skin	Deep	Skin	Deep	Skin	Deep	Skin	Deep
^{11}C	8.88E-01	2.35E-01	2.99E-02	1.41E-02	3.24E-03	1.97E-03	1.05E-03	7.42E-04	2.25E-04	1.93E-04
^{13}N	1.43E+00	2.38E-01	4.63E-02	1.42E-02	5.01E-03	1.94E-03	1.63E-03	7.47E-04	2.90E-04	1.94E-04
^{15}O	3.23E+00	3.02E-01	1.01E-01	1.49E-02	1.11E-02	2.00E-03	3.77E-03	7.66E-04	7.58E-04	1.98E-04
^{18}F	5.77E-01	2.17E-01	2.07E-02	1.37E-02	2.50E-03	1.86E-03	8.47E-04	7.15E-04	2.06E-04	1.85E-04
^{22}Na	1.35E+00	4.56E-01	3.51E-02	2.77E-02	4.33E-03	3.62E-03	1.62E-03	1.35E-03	4.03E-04	3.55E-04
^{24}Na	3.33E+00	7.03E-01	8.40E-02	3.99E-02	9.67E-03	5.07E-03	3.36E-03	1.88E-03	7.65E-04	4.87E-04
^{32}P	2.62E+00	7.69E-02	7.56E-02	5.11E-05	7.98E-03	7.49E-06	2.70E-03	3.13E-06	5.20E-04	7.80E-07
^{41}Ar	1.49E+00	2.65E-01	4.35E-02	1.45E-02	4.93E-03	1.86E-03	1.67E-03	6.99E-04	3.41E-04	1.77E-04
^{44}Sc	2.78E+00	4.85E-01	8.27E-02	2.76E-02	9.16E-03	3.61E-03	3.16E-03	1.37E-03	6.58E-04	3.54E-04
^{51}Cr	[illegible]	[illegible]	[illegible]	[illegible]	[illegible]	[illegible]	[illegible]	[illegible]	[illegible]	[illegible]

- *E. Amato, A. Italiano, L. Auditore, S. Baldari.*
- **Radiation protection from external exposure to radionuclides: A Monte Carlo data handbook**.
- *Physica Medica 46 (2018) 160*

Organ-level internal dosimetry on anthropomorphic phantoms

$$\bar{D}_{s\to t} = \frac{\tilde{A}_s}{m_t} E_{\text{dep}} = \frac{\tilde{A}_s\left(\Delta_\beta \varphi_\beta + \sum_i \; p_i \, E_i \varphi_{\gamma_i}\right)}{m_t} = \tilde{A}_s S_{s\to t}$$

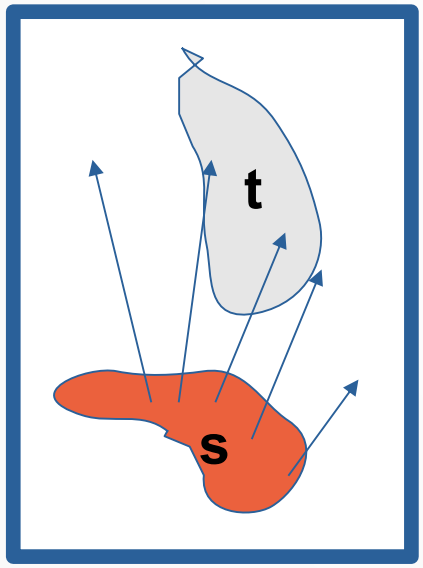

$$D(r_k \leftarrow r_h) = \tilde{A}_h S(r_k \leftarrow r_h)$$

$$D(r_k) = \sum_h \tilde{A}_h \sum_i \Delta_i \Phi_i (r_k \leftarrow r_h) / m_h$$

Anthropomorphic phantoms

Adult and pediatric phantoms:

- ICRP (ICRP 110...)
- MIRD
- ORNL
- Cristy & Eckermann
- Kramer

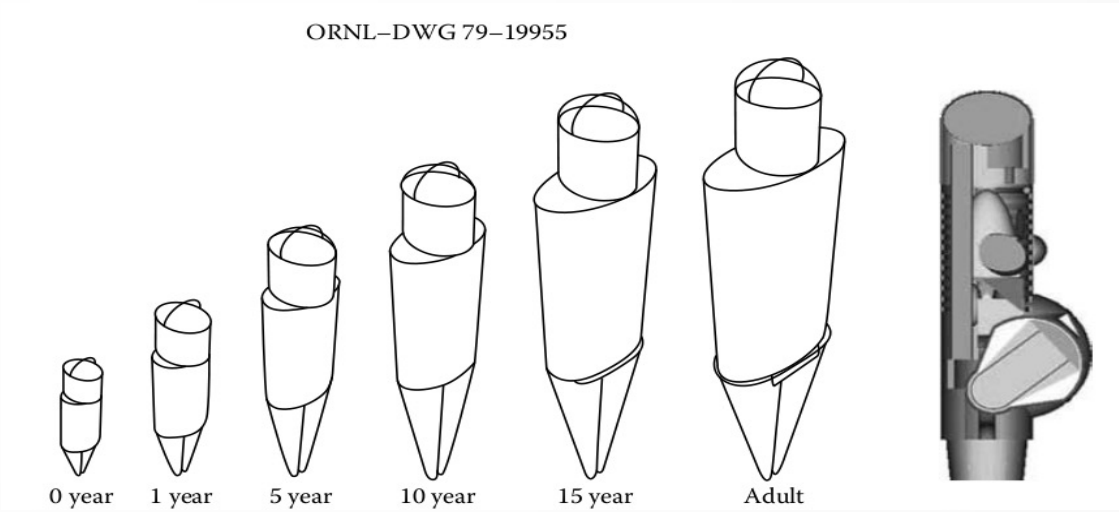

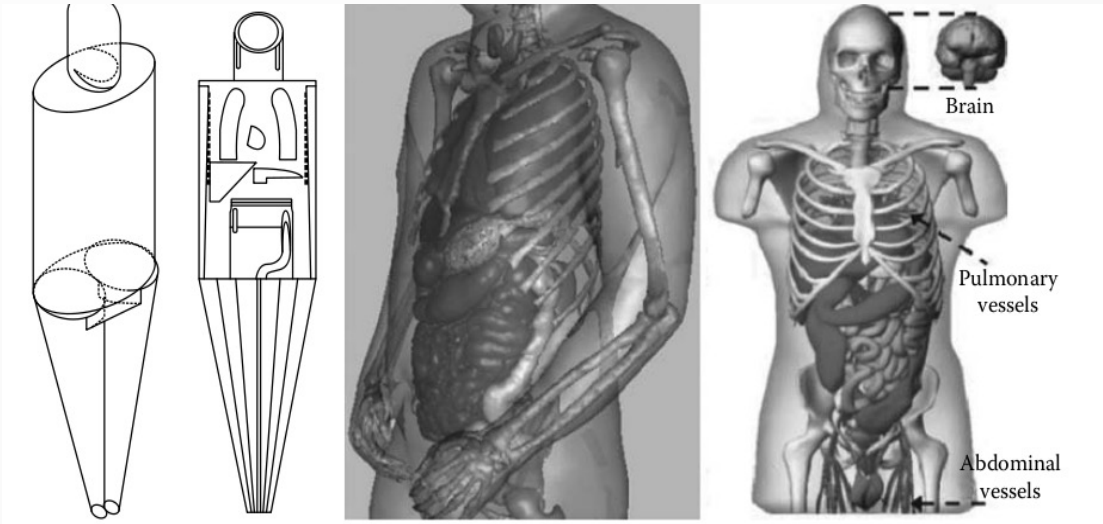

Handbook of anatomical models for radiation dosimetry,
Ed. Xu & Eckermann, CRC Press

MIRD schema: organ S factors

TABLE B13
S Values for Sources Located in the Thyroid

Targets	S values (mGy · MBq^{-1} sec^{-1})											
	^{99m}Tc	^{122}I	^{123}I	^{124}I	^{125}I	^{125m}I	^{126}I	^{130}I	^{131}I	^{132}I	^{132m}I	^{133}I
Brain (total)	1.03E − 07	8.81E − 07	1.27E − 07	9.78E − 07	5.61E − 09	3.96E − 07	4.54E − 09	2.01E − 06	3.45E − 07	2.12E − 06	2.94E − 07	5.68E − 07
Caudate nuclei	1.41E − 07	1.18E − 06	1.75E − 07	1.25E − 06	5.88E − 09	5.25E − 07	4.86E − 09	2.63E − 06	4.73E − 07	2.71E − 06	3.84E − 07	7.53E − 07
Cerebellum	8.81E − 08	7.94E − 07	1.09E − 07	8.84E − 07	2.37E − 09	3.56E − 07	2.24E − 09	1.82E − 06	3.08E − 07	1.92E − 06	2.65E − 07	5.13E − 07
Cerebral cortex	9.35E − 08	8.29E − 07	1.16E − 07	9.20E − 07	5.30E − 09	3.73E − 07	4.24E − 09	1.90E − 06	3.23E − 07	2.00E − 06	2.78E − 07	5.36E − 07
Cranium	1.57E − 07	8.51E − 07	1.82E − 07	9.47E − 07	2.38E − 08	3.93E − 07	1.81E − 08	1.94E − 06	3.58E − 07	2.04E − 06	2.94E − 07	5.47E − 07
Eyes	1.14E − 07	1.21E − 06	1.47E − 07	1.33E − 06	1.28E − 09	5.32E − 07	1.43E − 09	2.72E − 06	4.61E − 07	2.84E − 06	3.93E − 07	7.75E − 07
Lentiform nuclei	1.82E − 07	1.43E − 06	2.25E − 07	1.54E − 06	1.24E − 08	6.38E − 07	9.80E − 09	3.18E − 06	5.78E − 07	3.29E − 06	4.68E − 07	9.11E − 07
Mandible	7.66E − 07	3.68E − 06	1.03E − 06	3.93E − 06	3.98E − 07	1.74E − 06	2.73E − 07	8.01E − 06	1.58E − 06	8.20E − 06	1.29E − 06	2.30E − 06
Other tissues	1.44E − 06	3.23E − 05	2.51E − 06	1.37E − 05	1.48E − 06	5.69E − 06	8.28E − 07	2.43E − 05	4.68E − 06	2.79E − 05	4.23E − 06	9.17E − 06
Skin	3.20E − 07	2.64E − 06	5.05E − 07	2.83E − 06	2.17E − 07	1.21E − 06	1.29E − 07	5.78E − 06	1.04E − 06	5.97E − 06	8.90E − 07	1.65E − 06
Spinal cord	9.80E − 07	7.14E − 06	1.27E − 06	7.47E − 06	2.03E − 07	3.20E − 06	1.45E − 07	1.56E − 05	2.92E − 06	1.60E − 05	2.34E − 06	4.49E − 06
Spinal skeleton	1.52E − 06	7.20E − 06	2.12E − 06	7.71E − 06	9.26E − 07	3.45E − 06	6.29E − 07	1.57E − 05	3.1[illegible]E − 06	1.61E − 05	2.56E − 06	4.49E − 06
Thalami	2.02E − 07	1.41E − 06	2.50E − 07	1.53E − 06	2.00E − 08	6.40E − 07	1.52E − 08	3.16E − 06	5.9[illegible]E − 07	3.29E − 06	4.70E − 07	9.00E − 07
Thyroid	1.58E − 04	6.66E − 03	2.91E − 04	1.61E − 03	2.14E − 04	1.24E − 03	5.35E − 04	2.79E − 03	1.6[illegible]E − 03	4.11E − 03	1.27E − 03	3.22E − 03
Trunk	5.60E − 08	4.52E − 07	7.71E − 08	4.61E − 07	2.05E − 08	1.92E − 07	1.31E − 08	9.35E − 07	1.68E − 07	9.80E − 07	1.42E − 07	2.68E − 07
White matter	1.09E − 07	9.14E − 07	1.34E − 07	1.02E − 06	5.99E − 09	4.11E − 07	4.86E − 09	2.08E − 06	3.60E − 07	2.20E − 06	3.05E − 07	5.90E − 07

- Snyder, et al. MIRD Pamphlet 11: S, Absorbed Dose per Unit Cumulated Activity for Selected Radionuclides and Organs. **1975**; Society of Nuclear Medicine, Reston, VA.
- Snyder,et al. MIRD Pamphlet #5 Revised: Estimates of Absorbed Fractions for Monoenergetic Photon Sources Uniformly Distributed in Various Organs of a Heterogeneous Phantom. **1969**; J Nucl Med Suppl Number 3

The effect of simplistic geometries

Lee et al. “The effect of unrealistic thyroid vertical position on thyroid dose in the MIRD phantom” Med. Phys. 2004, 31:2038

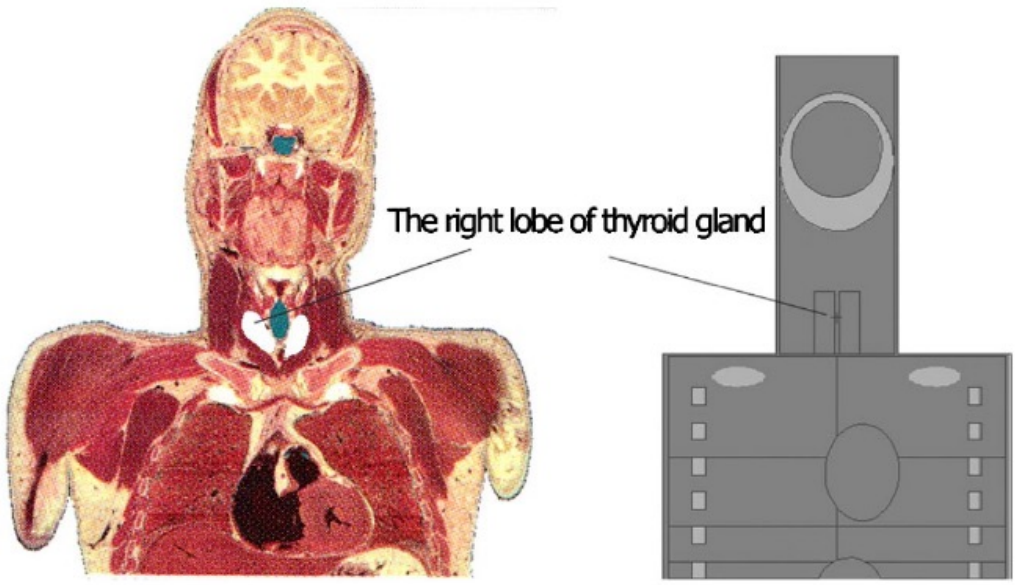

FIG. 1. Different positions of the thyroid gland in coronal views of Visual Human Male (white-colored) (left) and the MIRD phantom (right). The vertical position of the thyroid in the MIRD phantom is higher than that of actual human body.

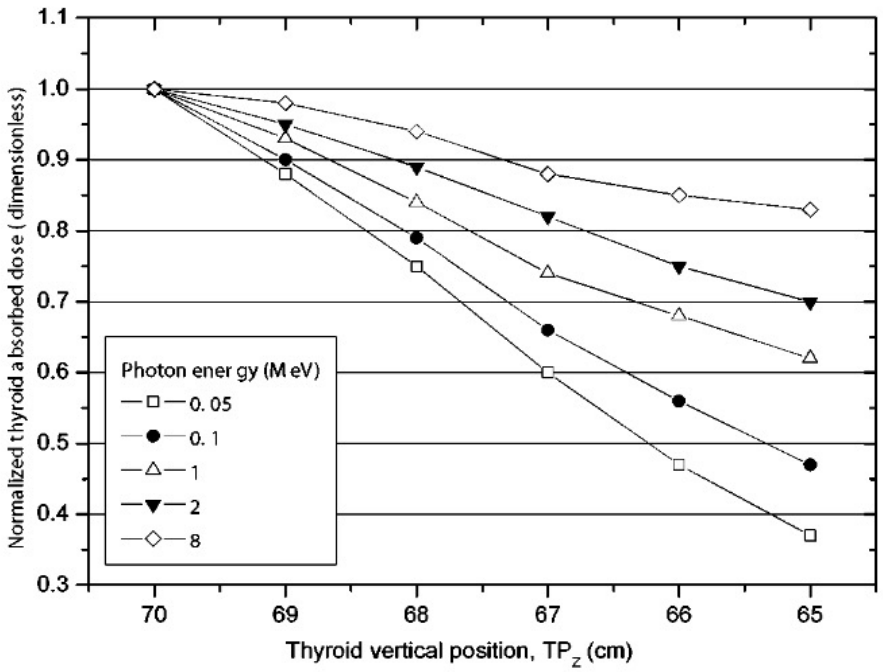

FIG. 3. The thyroid absorbed dose in RLAT geometry, normalized to the dose at $TP_Z = 70$ cm. $TP_Z = 70$ means the original position, and $TP_Z = 65$ means a complete insertion into the torso region.

Dosimetry of choroid plexuses

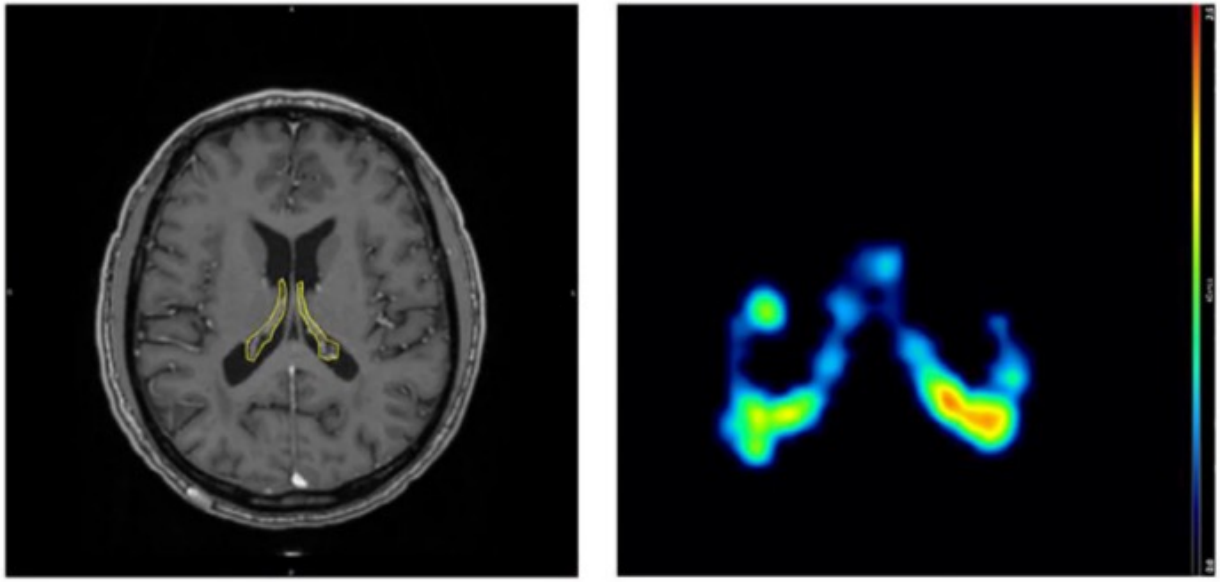

Fig. 1. a) An example of manual segmentation on axial T1-weighted MRI images of patient #1; b) Maximum intensity projection image of the choroid plexuses of patient #1, 60 min after the intravenous administration of ^{68}Ga-NODAGA-RGDyk; c) Three-dimensional volume of the choroid plexuses of patient #1; d) Tracks of 1.5-MeV electrons originating from the choroid plexuses (blue) and related bremsstrahlung photons (magenta), resulting from the Monte Carlo representation. Note that only the choroid plexuses of the lateral ventricles were contoured. (For interpretation of the references to colour in this figure legend, the reader is referred to the web version of this article.)

a) b)

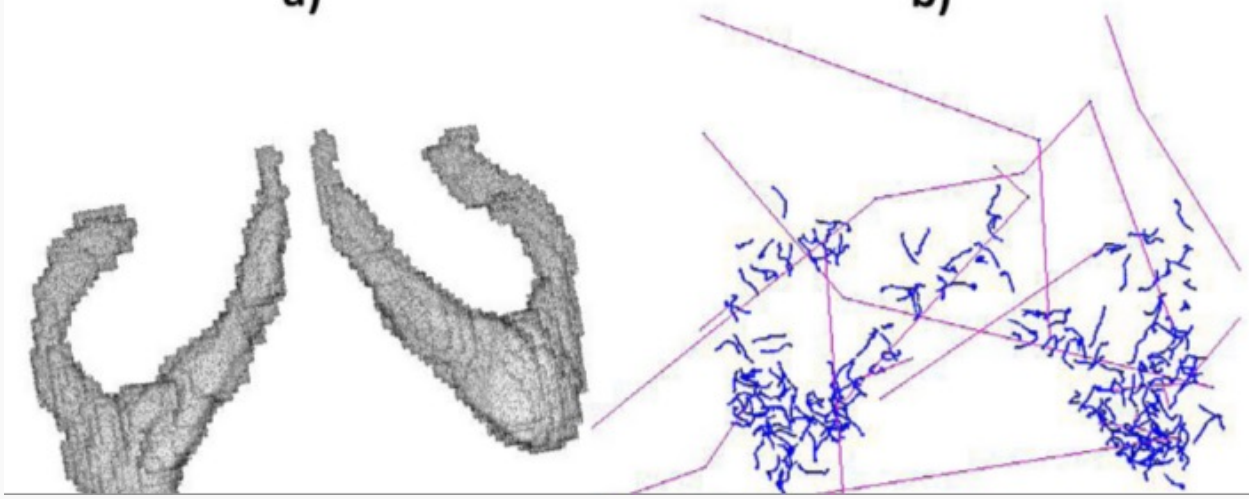

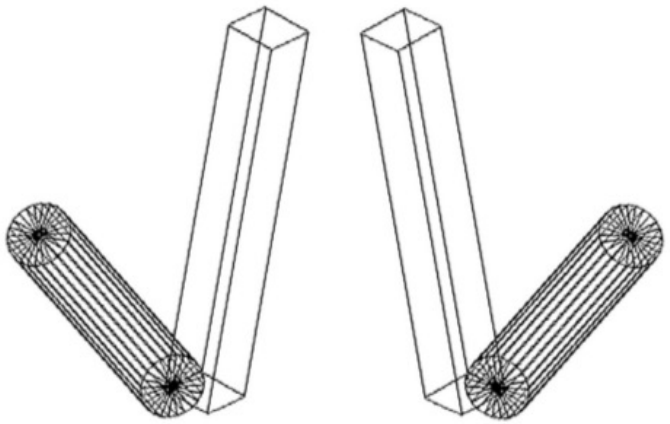

Fig. 2. Three-dimensional representation of the simplified geometrical model.

Amato, E., Cicone, F., Auditore, L., Baldari, S., Prior, J.O., Gnesin, S.
A Monte Carlo model for the internal dosimetry of choroid plexuses in nuclear medicine procedures (2018) Physica Medica, 49, 52-57.

OpenDose

https://www.opendose.org 90%

OpenDose Beta version

Newsletter Contact

- ISOTOPES
- MODELS
- SIMULATIONS
- SAFs
- S VALUES
- DOSIMETRY

Documentation

- The project
- The collaboration
- Publications and presentations
- Education

OpenDose software (coming soon)

- Model-based dosimetry

OpenDose

... open access resources for radiopharmaceutical dosimetry

The OpenDose collaboration brings together the resources and expertise of research teams involved in nuclear medicine dosimetry [1].

We aim to facilitate the practice of dosimetry in Nuclear Medicine by providing:

- Data (SAFs and S values).
- Software (model-based and patient-specific dosimetry). Work in progress...
- Education material (lectures and recommended readings).

You can find information on the project and collaboration from the documentation section:
the project, the collaboration and publications and presentations.

[1] OpenDose: open access resources for nuclear medicine dosimetry. Journal of Nuclear Medicine, 2020.

News

13-03-2020 - OpenDose article published in the Journal of Nuclear Medicine

Title: OpenDose: open access resources for nuclear medicine dosimetry.
Authors: Maxime Chauvin, Damian Borys, Francesca Botta, Pawel Bzowski, Jérémie Dabin, Ana M Denis-Bacelar, Aurélie Desbrée, Nadia Falzone, Boon Quand Lee, Andrea Mairiani, Alessandra Malaroda, Gilles Mathieu, Erin McKay, Erick Mora-Ramirez, Andrew P Robinson, David Sarrut, Lara Struelens, Alex Vergara Gil and Manuel Bardiès for the OpenDose collaboration.
https://doi.org/10.2967/jnumed.119.240366

www.opendose.org

OpenDose Beta version

Newsletter

- ISOTOPES
- MODELS
- SIMULATIONS
- SAFs
- S VALUES
- DOSIMETRY

Selection

Model ICRP 110 AF

Region Brain

Submit

Models

You can select a region from the left panel to highlight it.

ICRP 110 AF

Height (m)	1.63
Mass (kg)	60
Number of voxels, x	299
Number of voxels, y	137
Number of voxels, z	348
Voxel size, x (mm)	1.775
Voxel size, y (mm)	1.775
Voxel size, z (mm)	4.84
Number of regions (including compound regions)	168

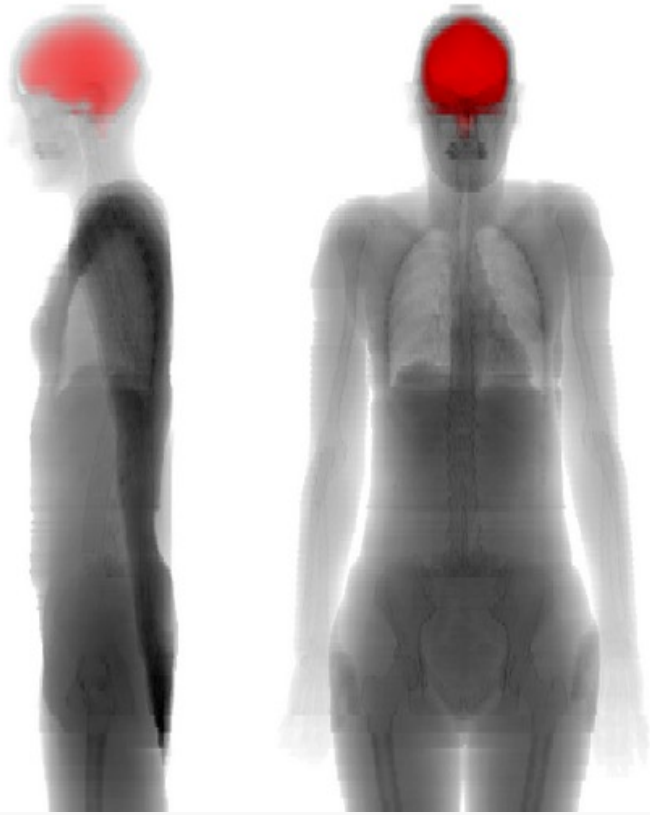

OpenDose

OpenDose Beta version

Newsletter Contact

- ISOTOPES
- MODELS
- SIMULATIONS
- SAFs
- S VALUES
- DOSIMETRY

Selection

Model ICRP 110 AF

Source Select a source

Isotope Select a radioisotope

Submit

S values

To display *S values*, first select a model from the left panel, then select a source and a radioisotope.

The *S values* calculated refer only to the radionuclide under consideration, so to evaluate the absorbed dose one must consider the decay and the *S values* of all the daughters.

S values are calculated following the equation:

$$S_{(Target \leftarrow Source)} = \sum_i y_i E_i \Phi_{i(Target \leftarrow Source)}$$

where $\Phi_{i(Target \leftarrow Source)}$ is the Specific Absorbed Fraction (SAF, kg^{-1}) for radiation type i and y_i, E_i are the yield ($Bq^{-1}.s^{-1}$) and energy (J) of radiation type i, respectively.

A Python program performs the calculation for a selected set of parameters (model, source, radioisotope). From the selection and for each target, the Python script queries all corresponding SAFs from the OpenDose database and the radioisotope decay data of ICRP publication 107 [1]. The SAFs are then averaged between all Monte Carlo codes and interpolated to each radiation type energy of the selected radioisotope. Then, the interpolated SAFs are multiplied by the yield and energy of this radiation type or interpolated over the beta spectrum. Finally, every radiation type contribution is summed to give the *S value*.

The *S value* statistical uncertainty is estimated following the equation:

$$\sigma\left(S_{(Target \leftarrow Source)}\right)^2 = \sum_i \left(y_i E_i \sigma\left(\Phi_{i(Target \leftarrow Source)}\right)\right)^2$$

where $\sigma\left(\Phi_{i(Target \leftarrow Source)}\right)$ is the SAF statistical uncertainty (kg^{-1}) for radiation type i and y_i, E_i are the yield ($Bq^{-1}.s^{-1}$) and energy (J) of radiation type i, respectively.

This section allows to get *S values* for 2 models, 141 sources, 172 targets and 1252 radioisotopes. An interactive chart shows *S values* for all targets per particle type contribution, with their statistical uncertainties. A table at the bottom of the page shows *S values* with their statistical uncertainties for all targets and the mass of the target. The data from the table can be easily downloaded in CSV format with a button placed on top of it.

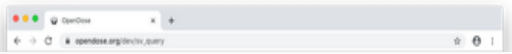

OpenDose

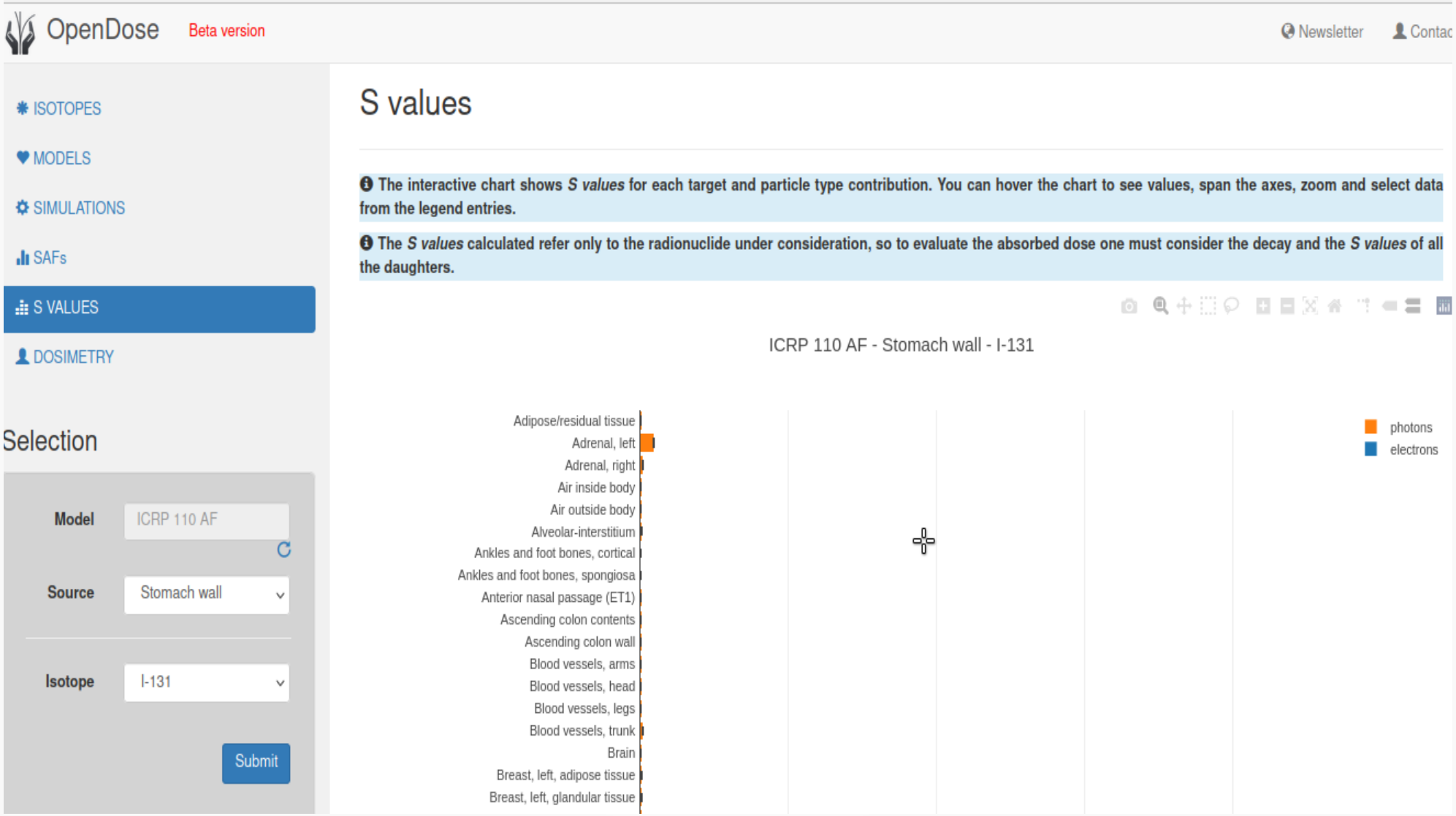
OpenDose
Beta version
Newsletter
Contac
ISOTOPES
MODELS
SIMULATIONS
SAFs
S VALUES
DOSIMETRY
S values
The interactive chart shows S values for each target and particle type contribution. You can hover the chart to see values, span the axes, zoom and select data from the legend entries.
The S values calculated refer only to the radionuclide under consideration, so to evaluate the absorbed dose one must consider the decay and the S values of all the daughters.
ICRP 110 AF - Stomach wall - I-131
Adipose/residual tissue
Adrenal, left
Adrenal, right
Air inside body
Air outside body
Alveolar-interstitium
Ankles and foot bones, cortical
Ankles and foot bones, spongiosa
Anterior nasal passage (ET1)
Ascending colon contents
Ascending colon wall
Blood vessels, arms
Blood vessels, head
Blood vessels, legs
Blood vessels, trunk
Brain
Breast, left, adipose tissue
Breast, left, glandular tissue
photons
electrons
Selection
Model
ICRP 110 AF
Source
Stomach wall
Isotope
I-131
Submit

Sphere model

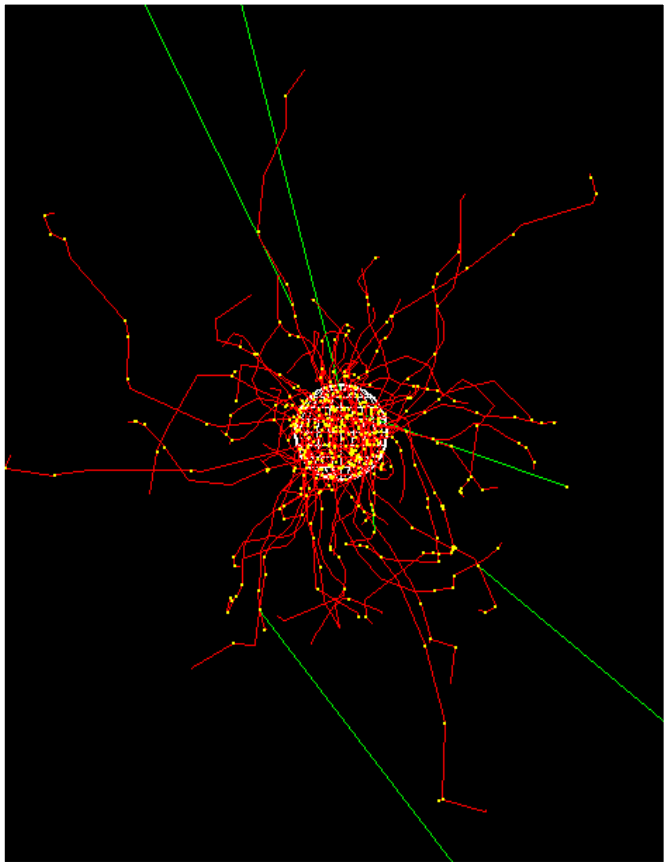

Absorbed fractions

$$\bar{D}_{s\to t} = \frac{\tilde{A}_s}{m_t} E_{\text{dep}} = \frac{\tilde{A}_s\left(\Delta_\beta \varphi_\beta + \sum_i p_i E_i \varphi_{\gamma_i}\right)}{m_t} = \tilde{A}_s S_{s\to t}$$

- Stabin and Konijnenberg "Re-evaluation of absorbed fractions for photons and electrons in spheres of various sizes" *J Nucl Med* 2000; **41**:149
- Bardies and Chatal "Absorbed doses for internal radiotherapy from 22 beta-emitting radionuclides: beta dosimetry of small spheres" *Phys Med Biol* 1994 **39**:961
- Bardies and Myers "A simplified approach to alpha dosimetry for small spheres labelled on the surface" *Phys. Med. Biol.* 1990 **35** 1551-61

Ellipsoidal model

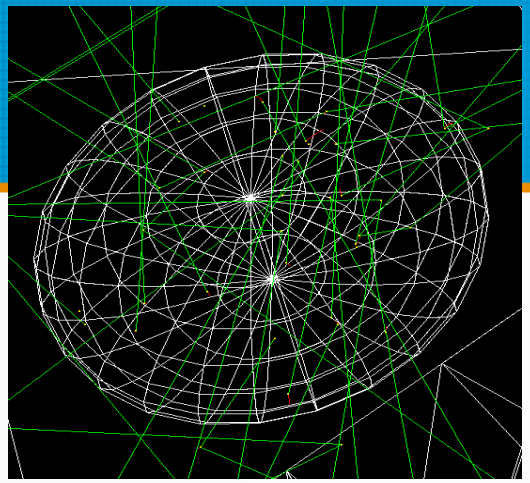

Prolate, oblate, scalene ellipsoids; spheres
Radiations: photons, beta and alpha particles

$$\rho = 3\frac{V}{S}$$

$$\varphi(\rho) = \left(1 + \frac{\rho_0}{\rho^s}\right)^{-1}$$

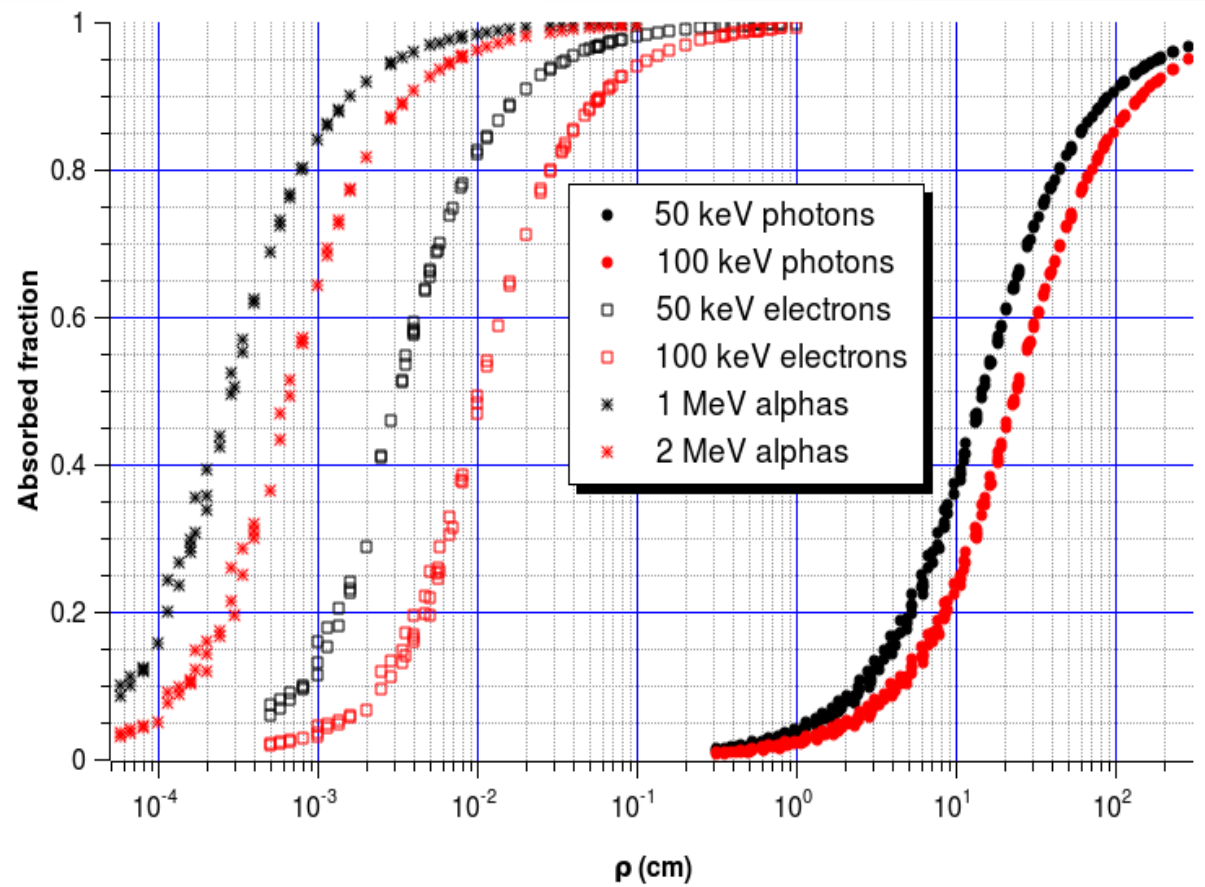

E. Amato, D. Lizio, S. Baldari, "Absorbed fractions for photons in ellipsoidal volumes", Phys. Med. Biol. **54** (2009) N479

E. Amato, D. Lizio, S. Baldari, "Absorbed fractions for electrons in ellipsoidal volumes", Phys. Med. Biol. **56** (2011) 357

E. Amato, A. Italiano, S. Baldari, "Absorbed fractions for alpha particles in ellipsoidal volumes", Phys. Med. Biol. **58** (2013) 5449

Analytic calculation of the self-dose in an ellpsoidal target

Semiaxes a, b, c → V and S → $3\frac{V}{S} = \rho$

$$\rho_0 = \rho_0(E)$$
$$s = s(E)$$

$$\varphi(\rho) = \left(1 + \frac{\rho_0}{\rho^s}\right)^{-1}$$

$$E_{\text{dep}} = \sum_i n_{\alpha,i} E_{\alpha,i} \varphi_{\alpha,i} + \int \frac{\text{dm}(E)}{\text{dE}} \text{E}\varphi(E)\text{dE} + \sum_i n_{\text{e},i} E_{\text{e},i} \varphi_{\text{e},i} + \sum_i n_{\gamma,i} E_{\gamma,i} \varphi_{\gamma,i}$$

$$\overline{D} = \text{D}_\alpha + \text{D}_\beta + \text{D}_\gamma = \frac{\tilde{A}}{m} E_{\text{dep}}$$

Implementaion in an electronic spreadsheet (177Lu example)

	A	B	C	D	E	F	G	H	I	J	K	L
1	Assi		semiassi (cm)									
2	1	cm	0,5	0,52	V (cm3)							
3	1	cm	0,5	3,14	S (cm2)					D beta	3,77E-02	mGy/MBqs
4	1	cm	0,5	0,5	rho (cm)					D Auger CE	4,08E-03	mGy/MBqs
5	1,04	dens. (g/cm3)								D X gamma	1,41E-04	mGy/MBqs
6												
7	E (keV)	p (%)	rho_0	s	phi	phi*E*p/100	X GAMMA			D totale	4,19E-02	mGy/MBqs
8	7,9	3,3	0,19	1,09	0,712	0,186						
9	54,61	1,64	35,96	1,28	0,011	0,010						
10	55,79	2,88	37,37	1,28	0,011	0,018						
11	63,2	1,21	45,32	1,29	0,009	0,007						
12	71,65	0,15	51,97	1,3	0,008	0,001				T residenza	1	Mbqh/MBq
13	112,95	6,4	59,3	1,27	0,007	0,050				A somm.	1	MBq
14	136,72	0,05	57,18	1,25	0,007	0,000						
15	208,37	11	50,54	1,2	0,009	0,195						
16	249,67	0,21	48,01	1,19	0,009	0,005				D terapia	0,2 Gy	
17	321,32	0,22	45,23	1,17	0,010	0,007						
18												
19						0,48	<Edep> (keV)					
20						1,41E-04	D (mGy/MBqs)					
21												
22	<Ebeta> (keV)		rho_0	s	phi	D (mGy/MBqs)	BETA					
23	132,9		0,017	1,099	0,96	3,77E-02						
24												
25	E (keV)	p (%)	rho_0	s	phi	phi*E*p/100	AUGER CE					
26	6,18	8,9	4,64E-05	0,88	1	0,550						
27	6,3	0,11	4,74E-05	0,89	1	0,007						
28	44,8	0,28	2,33E-04	1,4	1	0,124						
29	47,6	5,2	2,65E-04	1,4	1	2,473						
30	60,38	0,02	4,56E-04	1,42	1	0,013						

ellissoide_Lu177

Voxel S factors (VSVs)

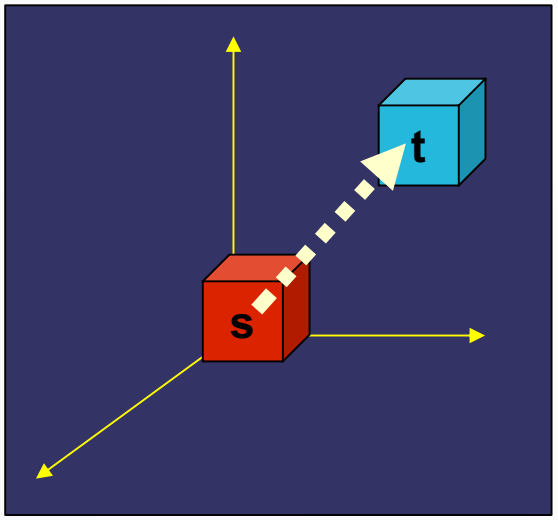

$$S_{k\leftarrow h} = \sum \Delta_i \cdot \frac{\varphi_i(k \leftarrow h)}{m_k}$$

MIRD Pamphlet no. 17

www.medphys.it

$$\bar{D}_k = \sum \tilde{A}_h \cdot S_{k\leftarrow h}$$

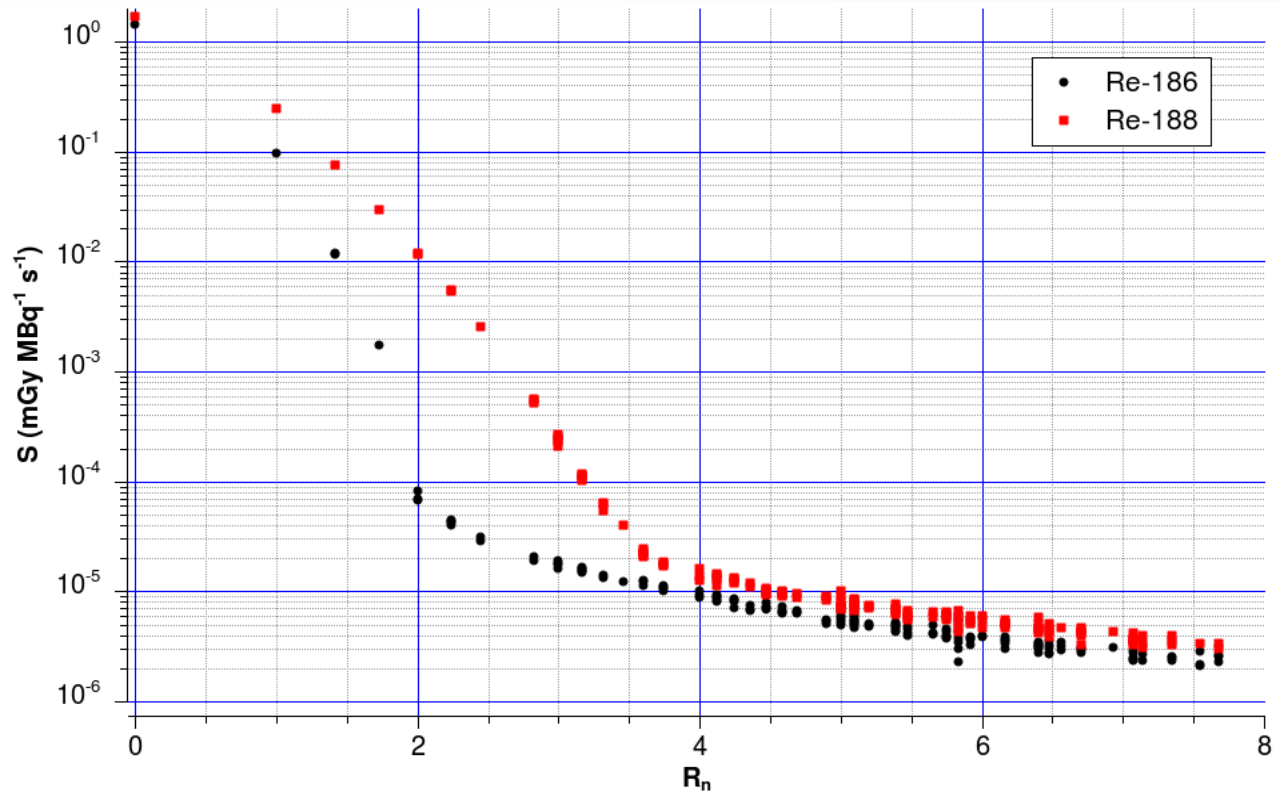

E. Amato *et al.* Nucl Instr Meth A 2013

Calculation of S factors for a generic l and electron spectrum

For monoenergetic electrons (E) in a given voxel side (l), S factors can be calculated interpolating the fit parameters at (E,l):

$$S_l(R_n) = \frac{E_{\text{dep,l}}(\text{E},\text{R}_n)}{m} \qquad R_n = \frac{R}{l} = \sqrt{i^2 + \text{j}^2 + \text{k}^2}$$

For a generic electron spectrum dn(E)/dE, S factors can be derived by integration:

$$S_l(R_n) = \frac{\langle E_{\text{dep}} \rangle}{m} = \frac{1}{m} \int \frac{\text{dn}(E)}{\text{dE}} E_{\text{dep,l}}(\text{E},\text{R}_n)\text{dE}$$

Monoenergetic electrons: 10-2000 keV

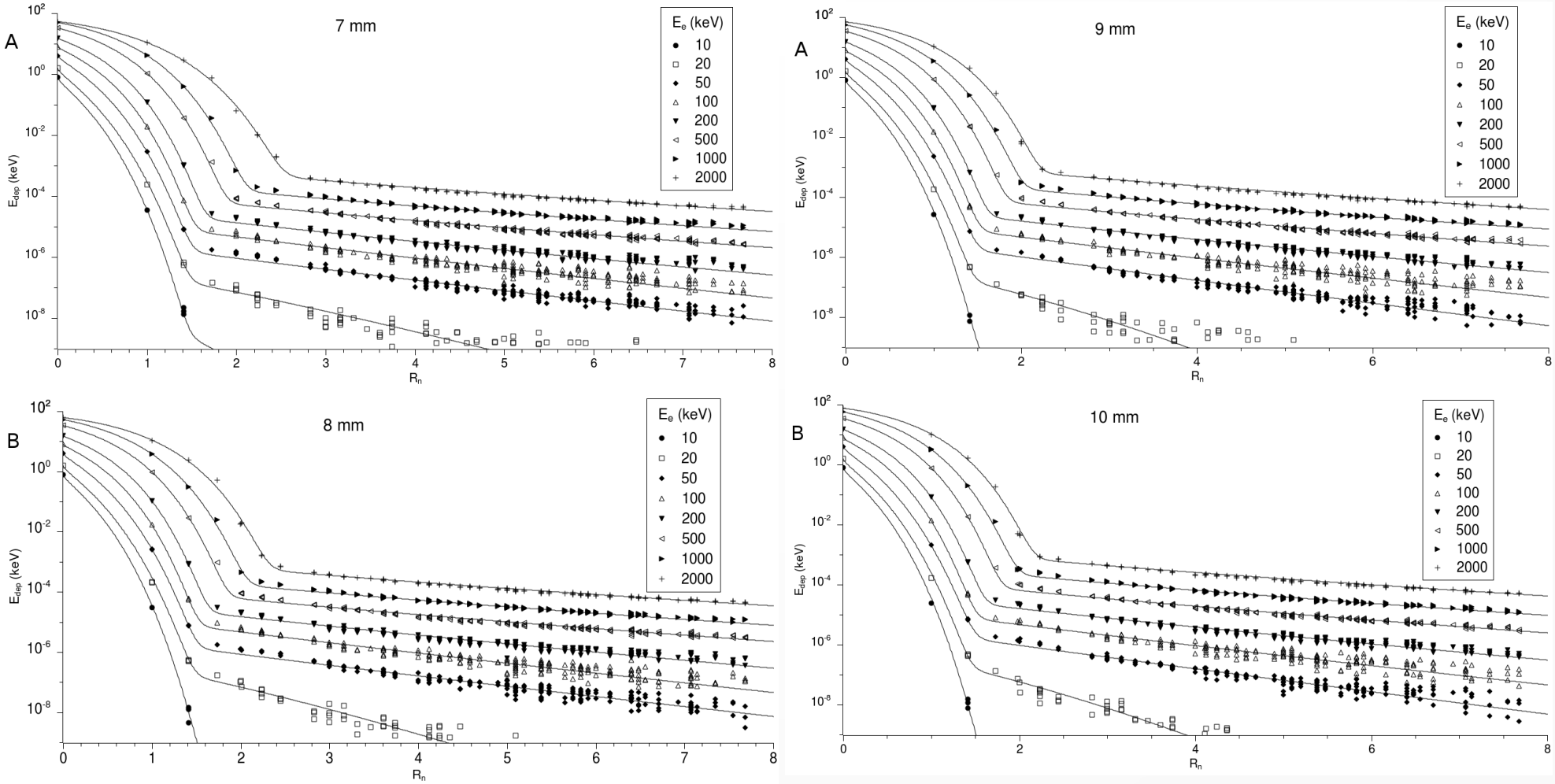

$$E_{\text{dep}}(R_n)=\text{aexp}\left(-\text{exp}(\text{bR}_n^c)\right)+\text{rexp}(-R_n^s)$$

Monoenergetic photons: 20-1000 keV

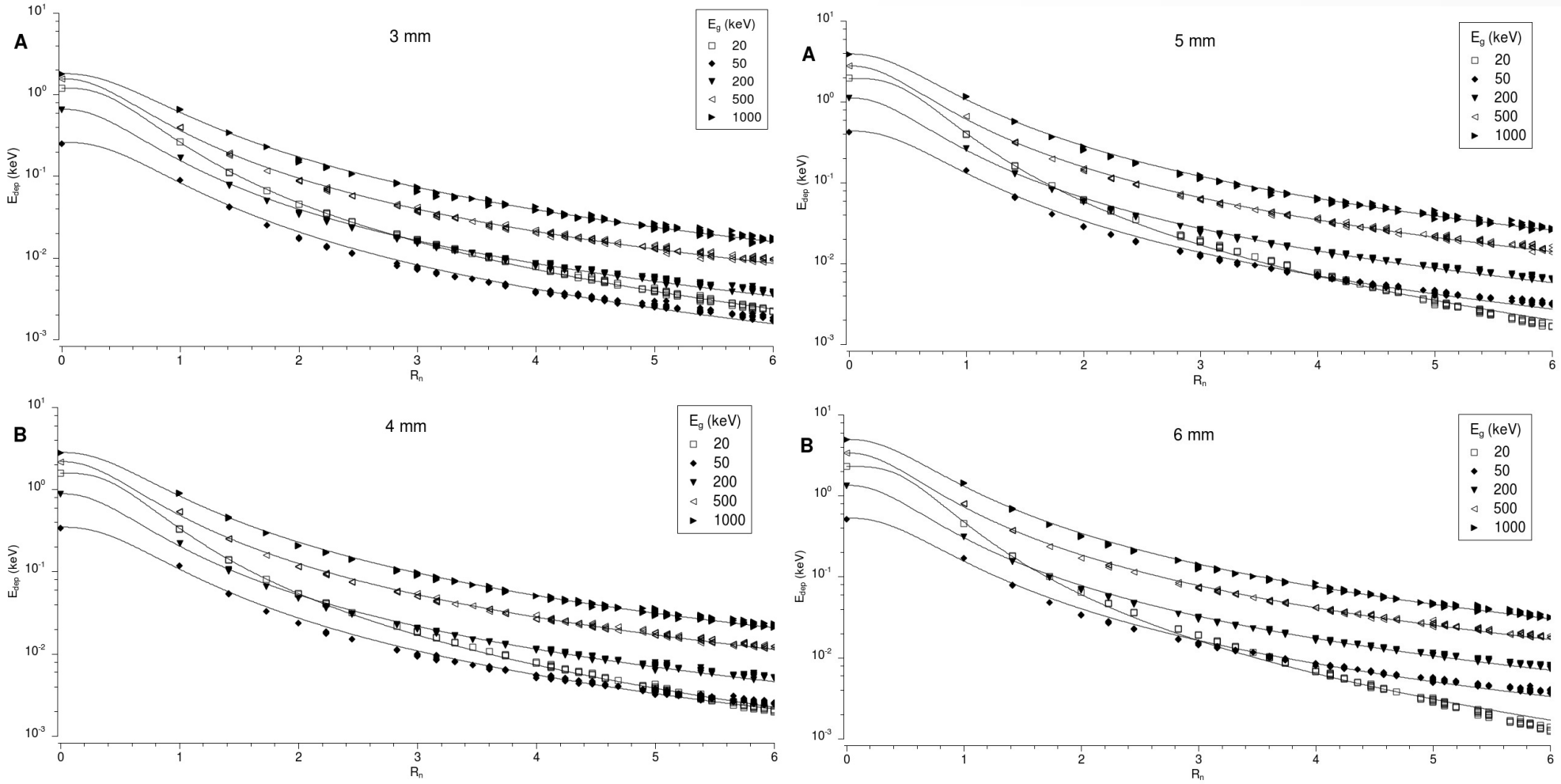

$$E_{\text{dep}}(R_n) = \frac{a}{R_n^b + c}$$

Calculation of S factors for a generic beta-gamma emitting radionuclide in a voxel of side l

$$S_l(R_n) = \frac{\langle E_{\mathrm{dep}} \rangle}{m} = \frac{1}{m}\left[\int \frac{\mathrm{dn}(E)}{\mathrm{dE}} E_{\mathrm{dep,l}}(\mathrm{E,R}_n)\mathrm{dE} + \sum \phi_i n_{\mathrm{e,i}} E_{\mathrm{dep,l}}(E_e,\mathrm{R}_n) + \sum \phi_j n_{\gamma,\mathrm{j}} E_{\mathrm{de}}\right.$$

Integration over the beta spectrum

Sum over the Auger and CE electrons

Sum over the X and gamma photons

E. Amato, F. Minutoli, M. Pacilio, A. Campennì, S. Baldari. "An analytical method for computing voxel S factors for electrons and photons" Med. Phys. **39 (11)** (2012) 6808-6817.

E. Amato, A. Italiano, F. Minutoli, S. Baldari. "Use of the GEANT4 Monte Carlo to determine three-dimensional dose factors for radionuclide dosimetry" Nucl. Instrum. Methods Phys. Res. A 708 (2013) 15-18

Dose Point Kernel (DPK)

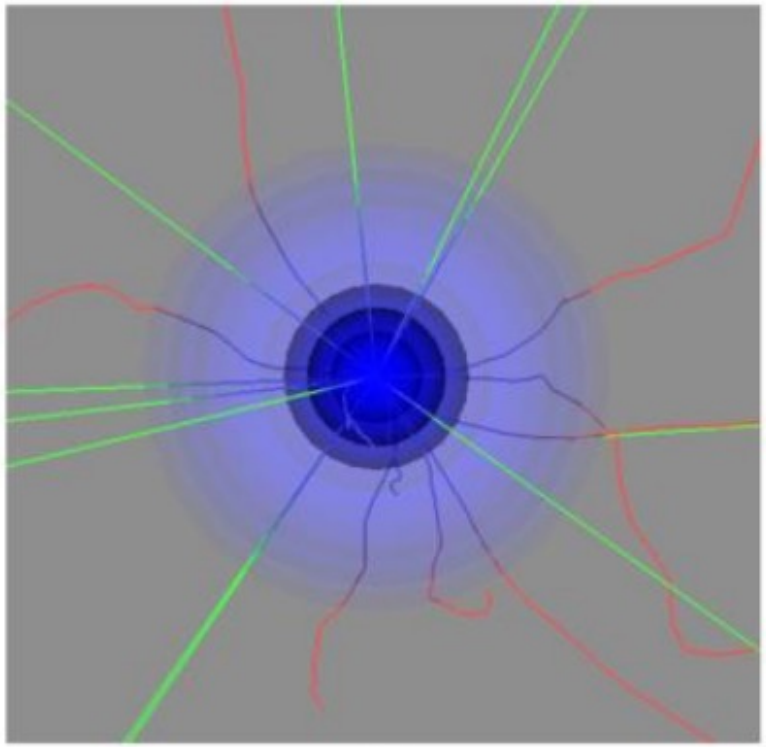

(a)

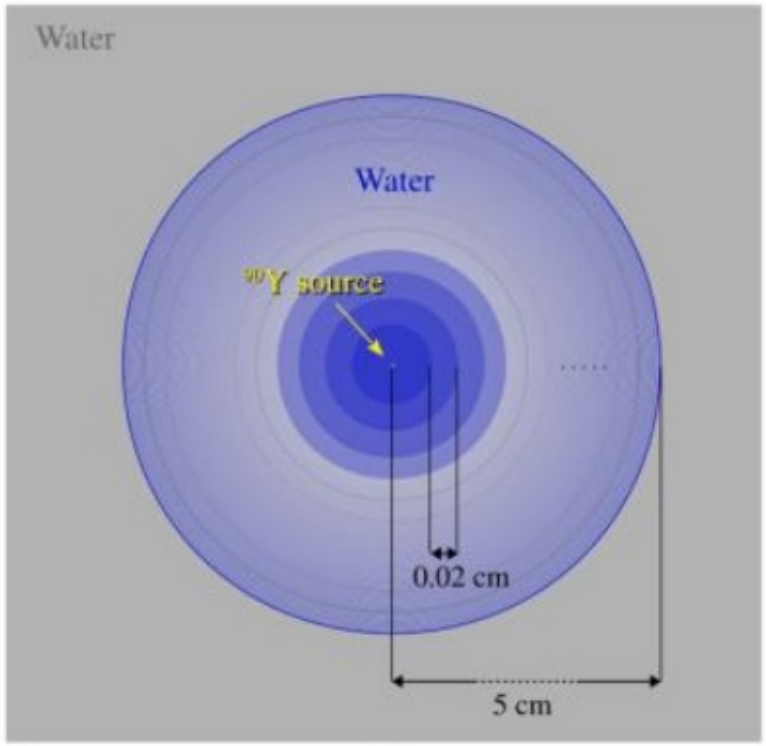

(b)

$$F_\beta(R/X_{90}) = 4\pi R^2 \rho X_{90} \phi_\beta(R)$$

$$\phi_\beta(R) = \frac{D(R)}{\bar{E}}$$

MC calculation of DPK for 90Y

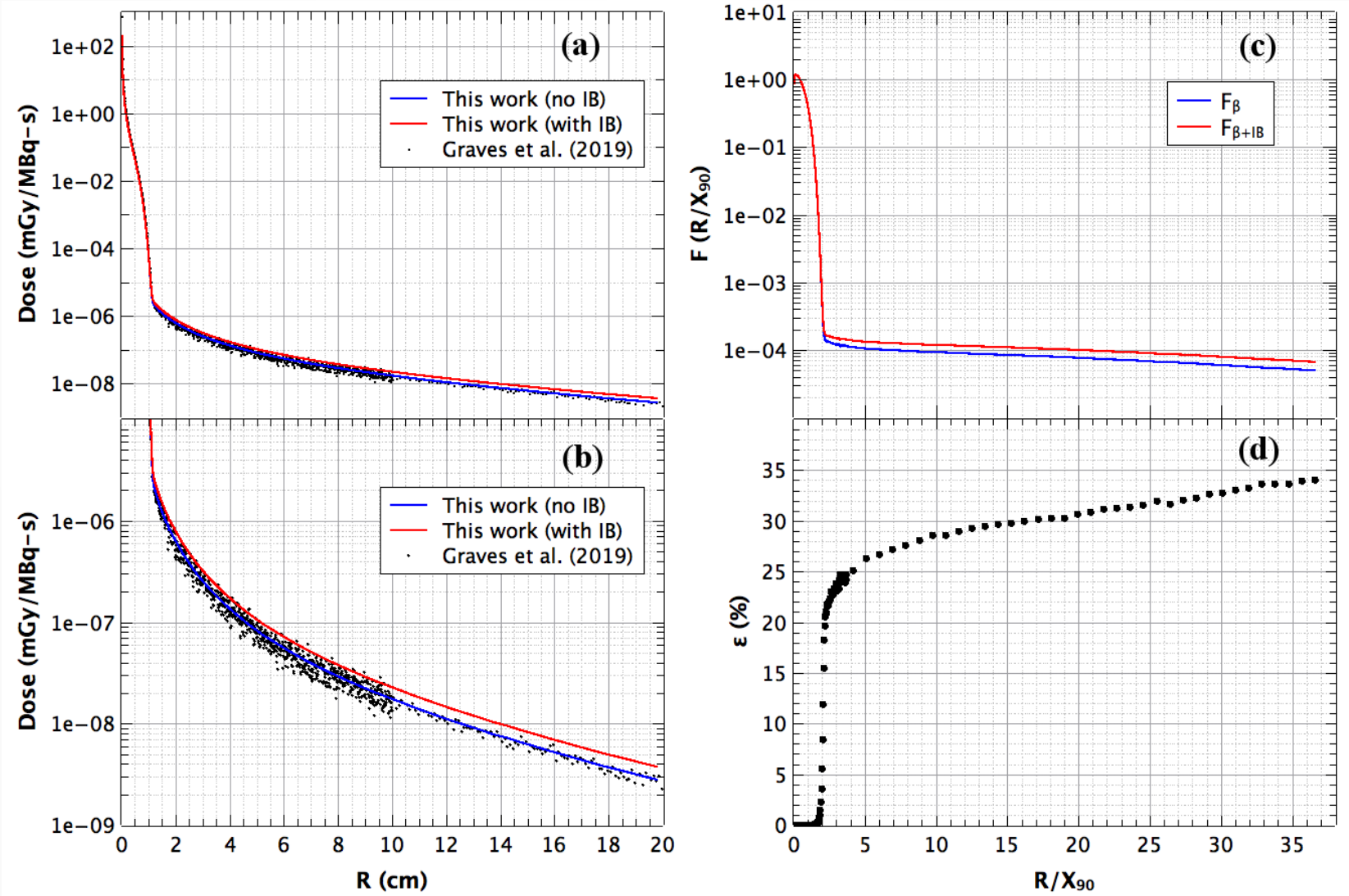

L. Auditore et al, The contribution of Internal Bremsstrahlung to the 90Y Dose Point Kernel, under revision

Direct MC Internal Dosimetry

Voxel level patient-specific direct Monte Carlo simulation

- Morphologic data:
  Computed Tomography (CT) scans
  (3D X-ray attenuation maps)
  → building voxelized phantoms

- Functional data:
  SPECT or PET scans
  (3D activity concentration maps)
  → building voxelized radionuclide spatial distributions

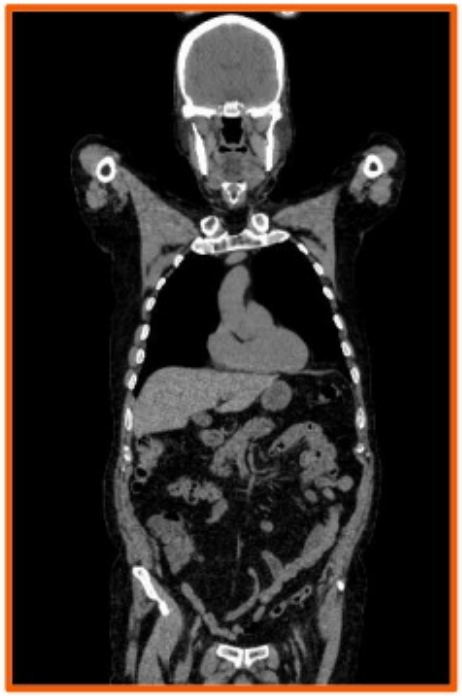

CT

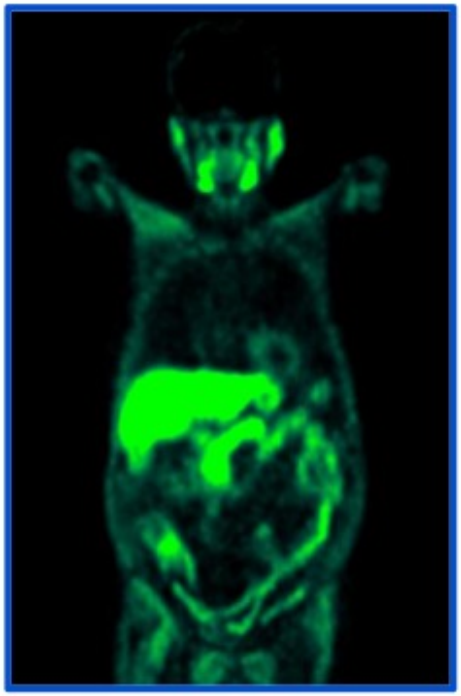

^{18}F-choline PET

Materials and density assignment

- Assign material (diff. chemical composition) from HU intervals
- Define submaterials (same chem. comp.) from HU subintervals
- Assign density to submaterials from HU-density relation

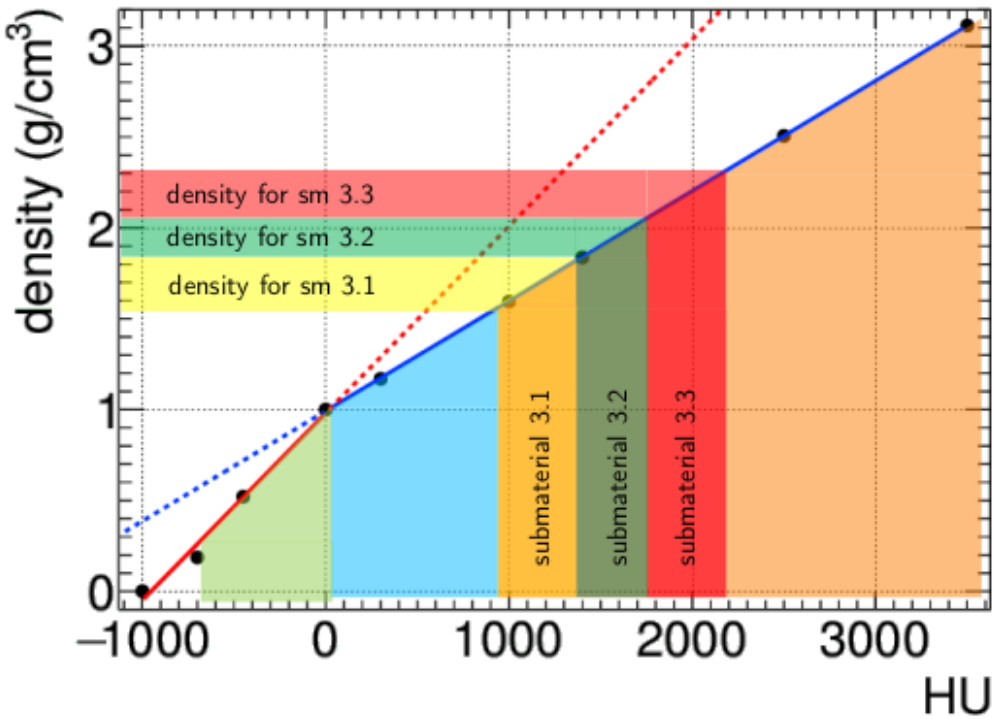

Hounsfield Units, also called CT numbers

Materials and density assignment

GAMOS

- Assign density directly converting through HU-density relation
- Assign material (chemical composition) from density intervals

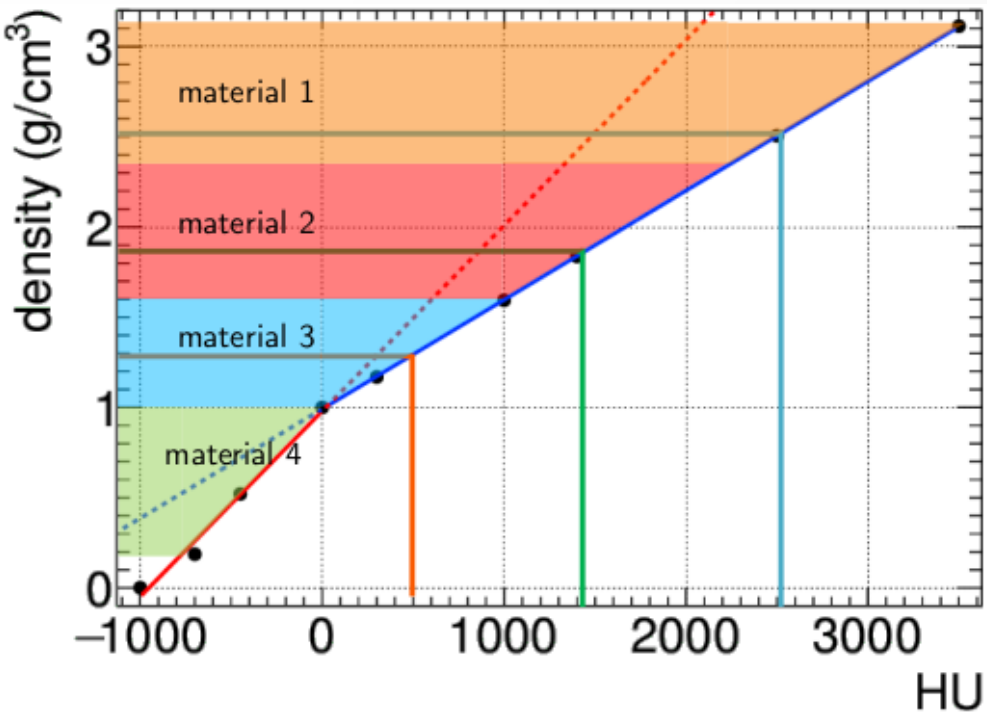

Hounsfield Units, also called CT numbers

Geometry from CT and Primaries from PET

Simulations setup

- Input data: co-registered ^{18}F-choline PET/CT

Philips Gemini TF 16 PET/CT scanner
Nuclear Medicine Unit, University Hospital "G. Martino", Messina

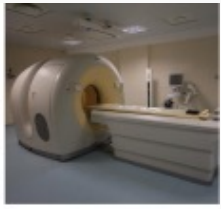

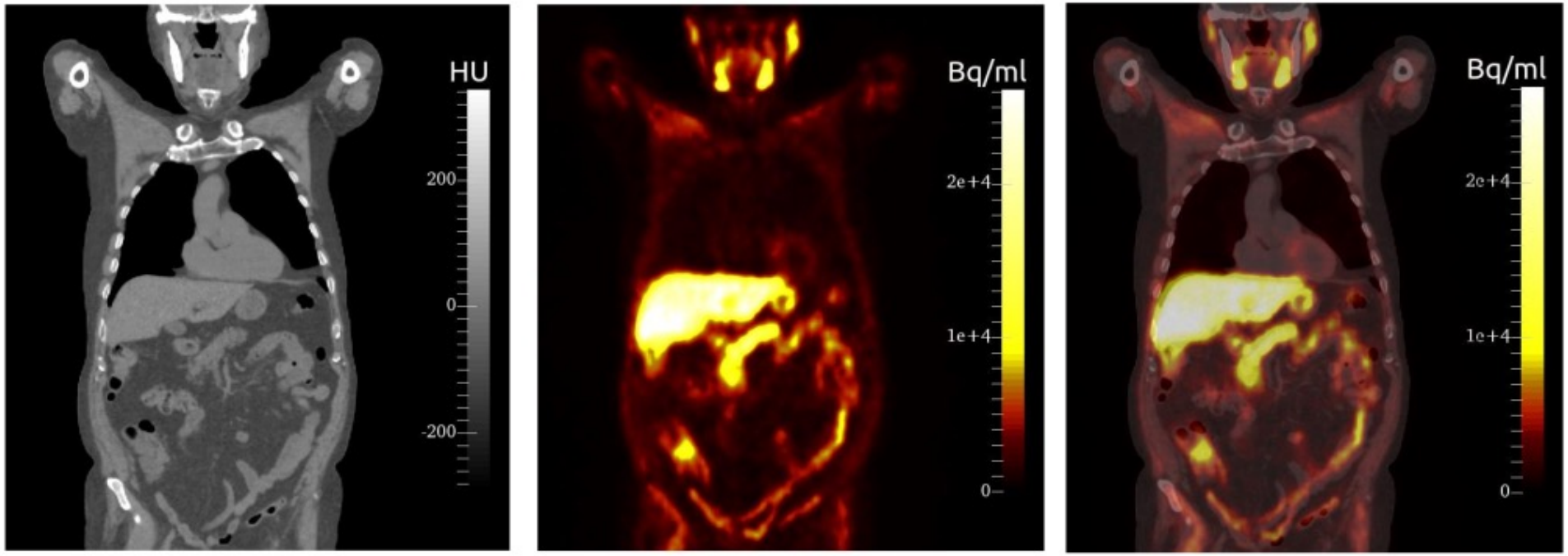

D. Pistone, et al. “Monte Carlo based dose-rate assessment in 18F-Choline PET examination: a comparison between GATE and GAMOS codes”.
Atti della Accademia Peloritana dei Pericolanti - Classe di Scienze Fisiche, Matematiche e Naturali, 98(1), p. A5, May 2020.

PET artifacts: motion blurirng, noise

Background and artifacts treamtent

- PET filtering technique
- Set $c_{A\ PET} = 0$ if $HU_{CT} < -855$ (setting zero decay probability in air)
- Require $c_{A\ PET} > 100$ Bq/ml (removing background noise)

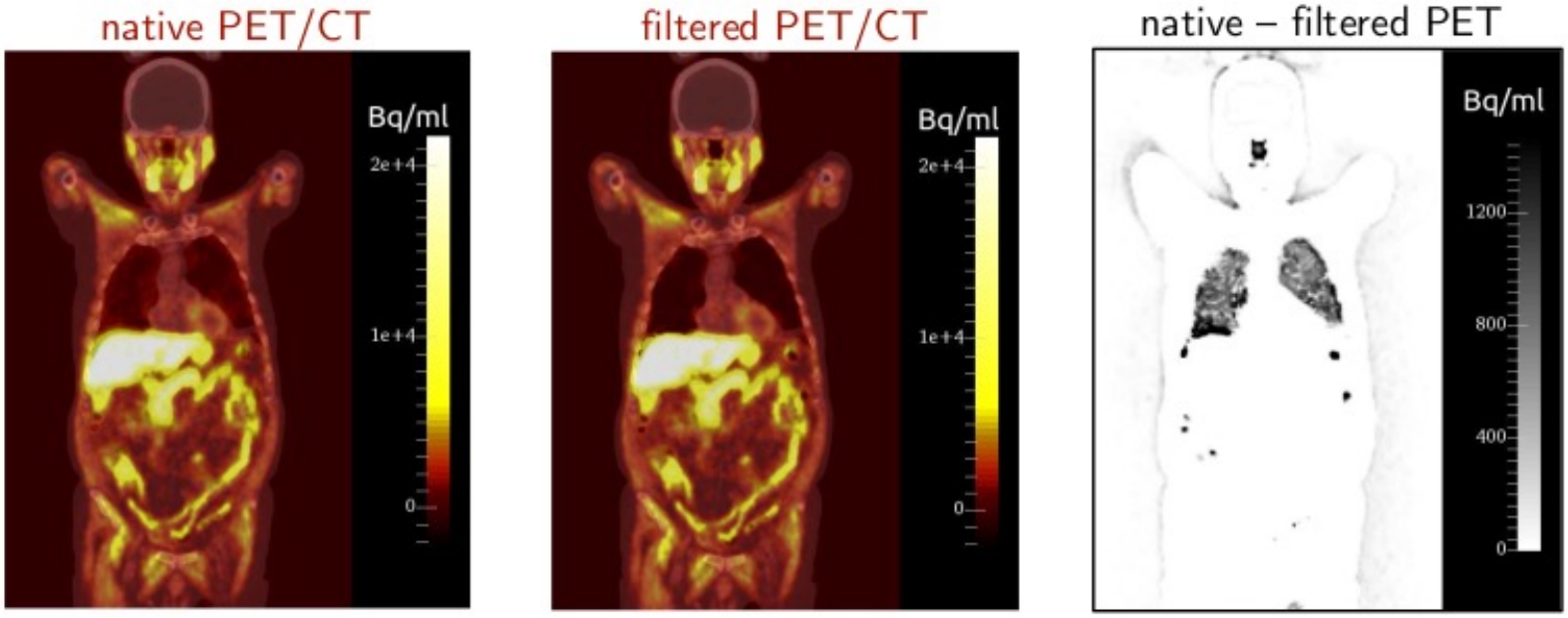

^{18}F-Choline MC dosimetry

Background and artifacts treamtent

- New simulations: same settings but using filtered PET images

Dose rate maps coronal slices

GATE simul. using native PET | GATE simul. using filtered PET | GATE simul. native - filtered

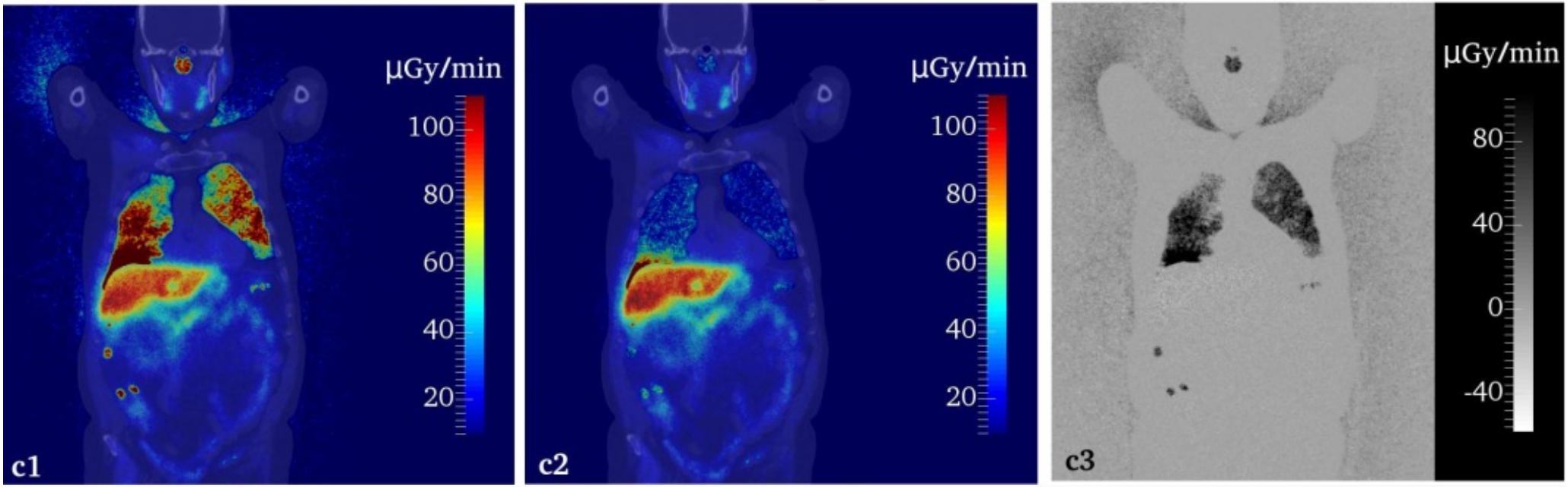

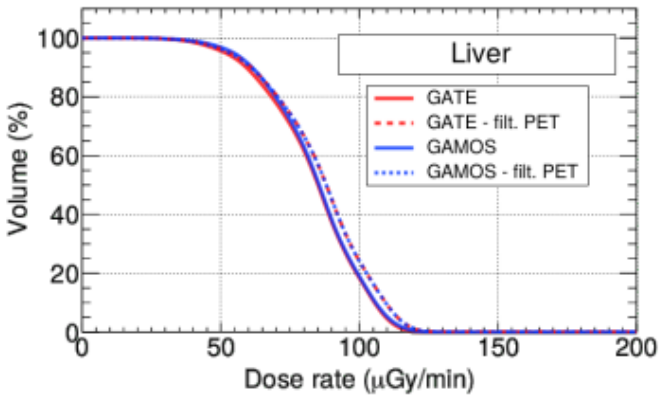

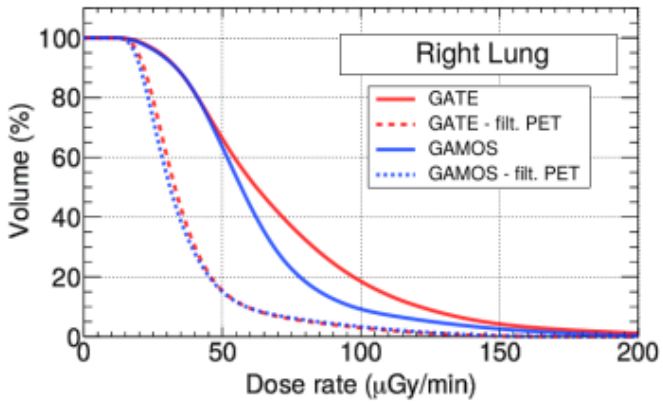

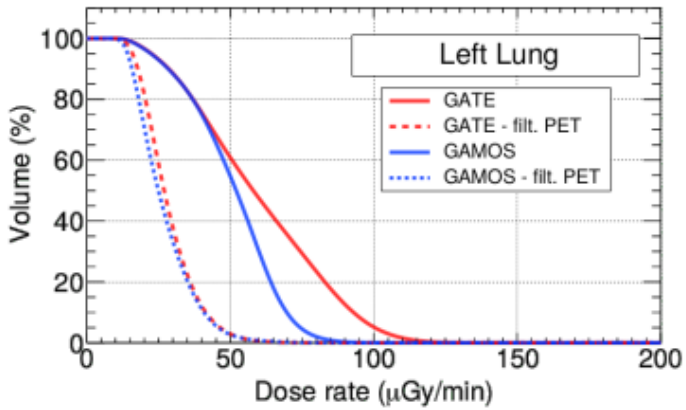

Small-scale internal dosimetry

- Kidneys
- Liver
- Pancreas
- Bone marrow
- Cell clusters
- Capillary vessels

Kidney anatomy

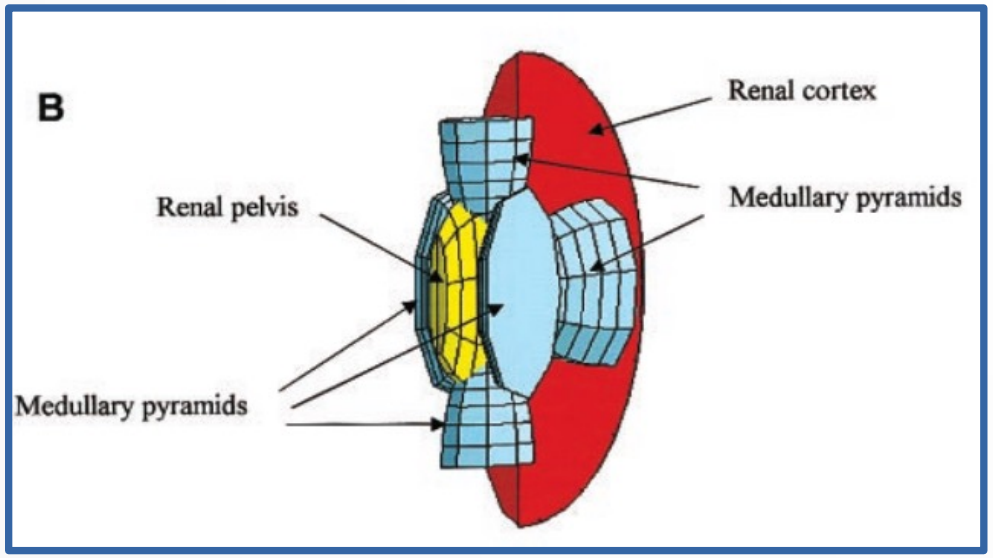

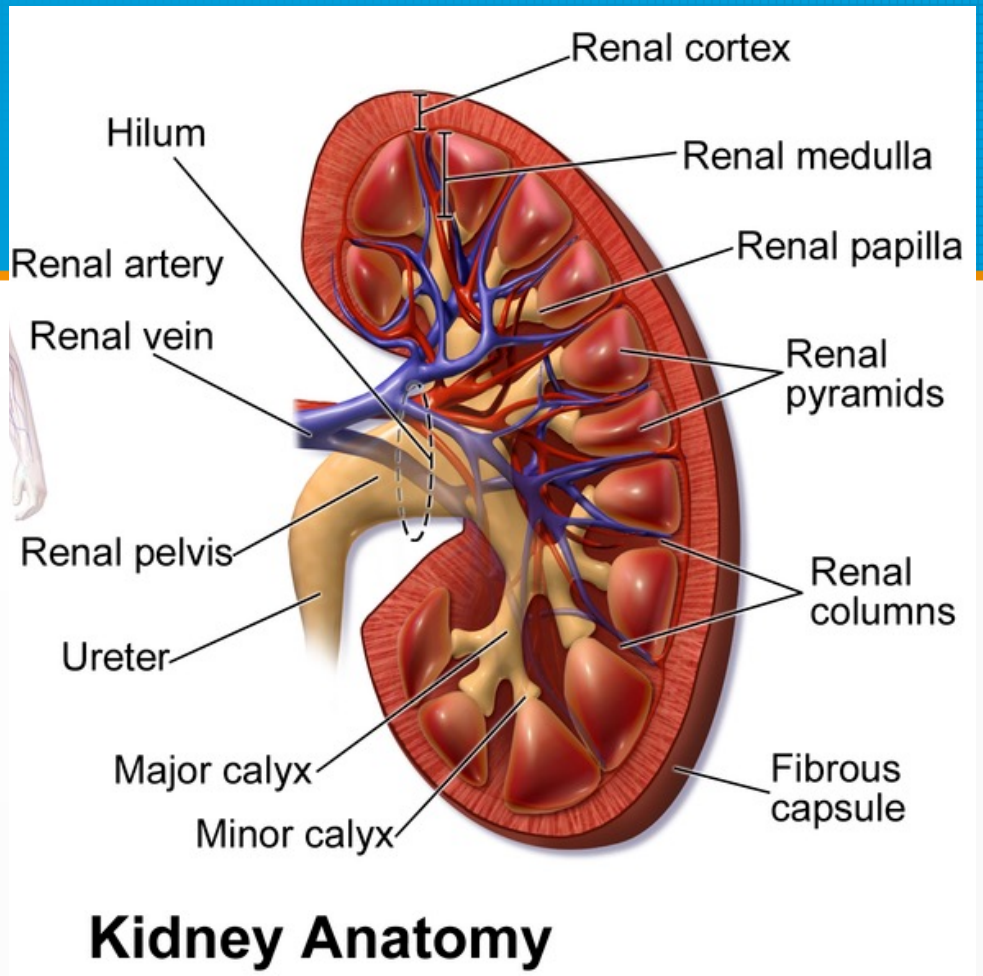

TABLE A22
Source Located in Renal Medulla of Adult

Targets	Photon absorbed fraction of energy Energy (MeV) 0.010	0.015	0.020	0.030	0.050	0.100	0.200	0.500	1.000	1.500	2.000	4.000
Cortex	1.23E−01	2.59E−01	2.72E−01	1.73E−01	7.37E−02	4.14E−02	4.12E−02	4.22E−02	3.91E−02	3.54E−02	3.26E−02	2.38E−02
Medulla	8.38E−01	5.90E−01	3.83E−01	1.67E−01	5.84E−02	3.36E−02	3.55E−02	3.70E−02	3.28E−02	2.79E−02	2.41E−02	1.46E−02
Pelvis	2.00E−02	4.10E−02	3.72E−02	2.06E−02	7.89E−03	4.53E−03	4.50E−03	4.69E−03	4.36E−03	4.00E−03	3.70E−03	2.44E−03
Papillae	1.30E−02	1.30E−02	1.00E−02	5.11E−03	1.85E−03	1.09E−03	1.06E−03	1.15E−03	1.03E−03	9.45E−04	8.25E−04	5.34E−04
Trunk	6.01E−03	9.59E−02	2.78E−01	5.02E−01	4.94E−01	3.75E−01	3.45E−01	3.37E−01	3.18E−01	2.99E−01	2.83E−01	2.38E−01

Targets	Electron absorbed fraction of energy Energy (MeV) 0.010	0.015	0.020	0.030	0.050	0.100	0.200	0.500	1.000	1.500	2.000	4.000
Cortex	0.00E+00	7.71E−05	1.49E−04	3.34E−04	8.07E−04	2.83E−03	9.28E−03	4.17E−02	1.13E−01	1.86E−01	2.43E−01	3.38E−01

Nephron model

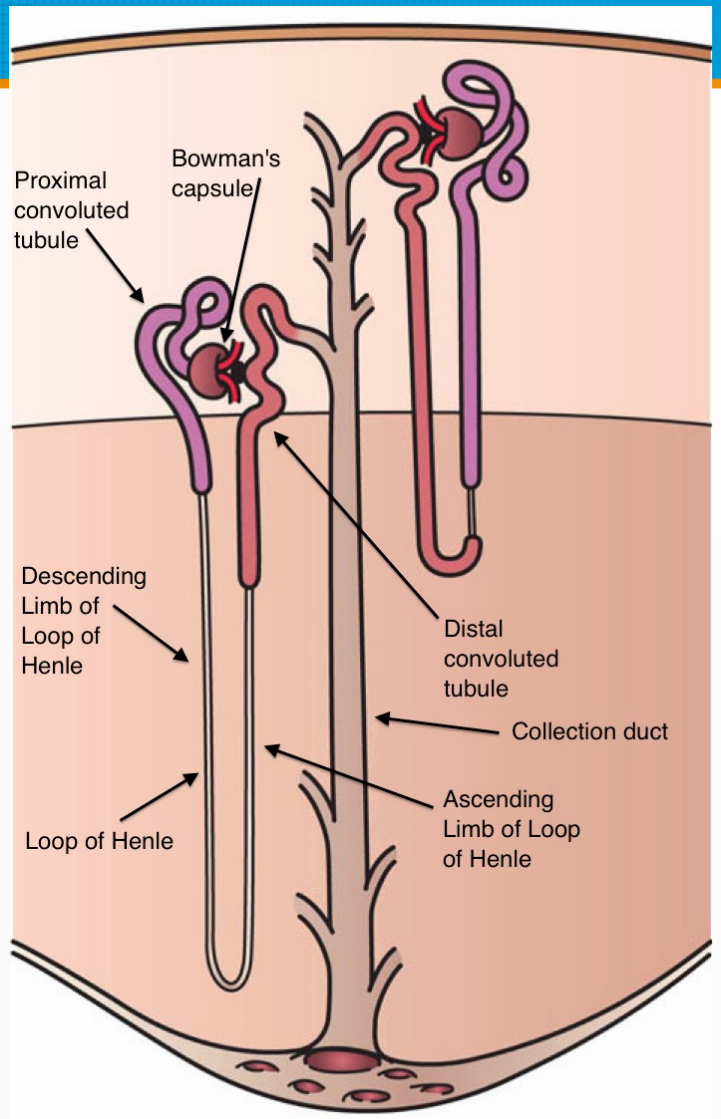

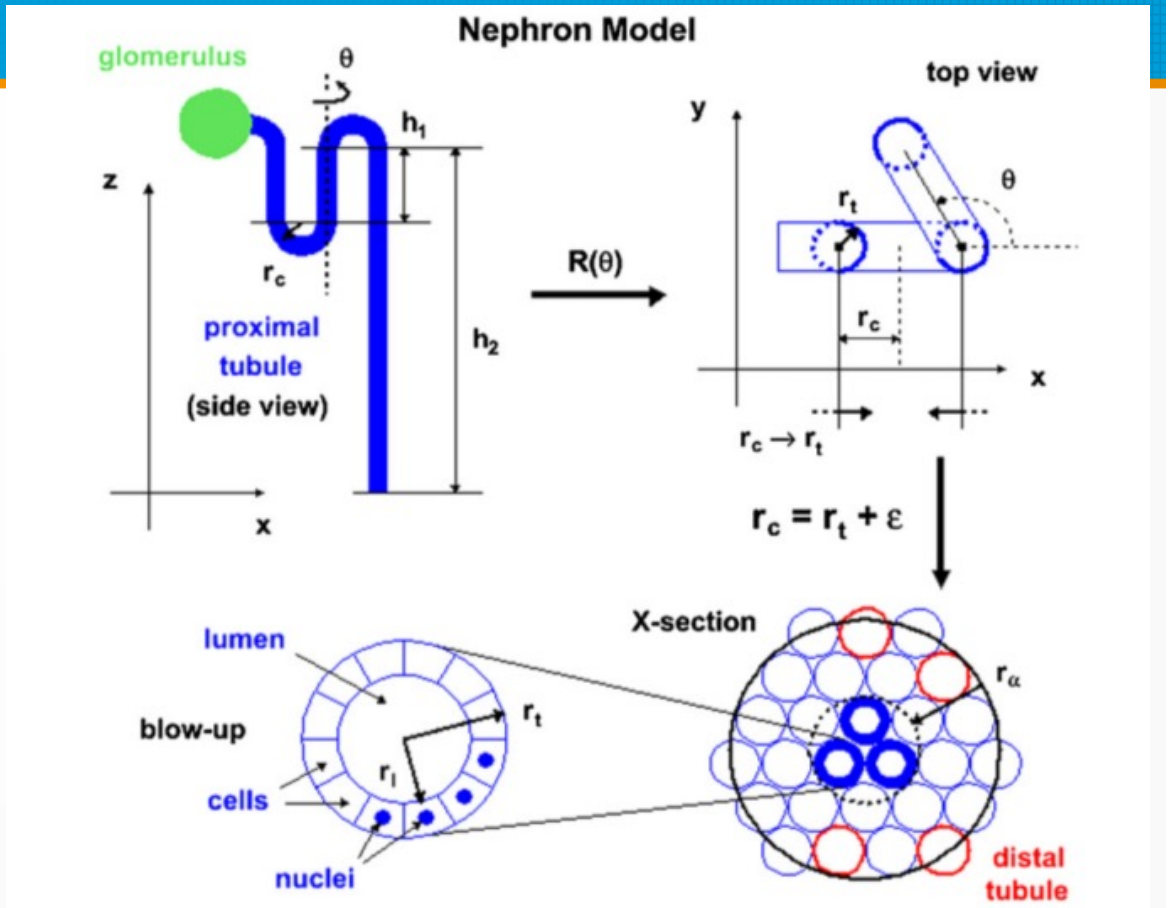

Figure 1. Idealized geometrical nephron model. The parameters shown are those used for the simulation: r_t is the proximal tubule radius, r_l is the lumen radius as measured by histology. The ε value is taken to be 1 μm and corresponds to interstitial space, h_1 and h_2 represent the scale of the proximal tubule length.

About 600.000 nephrons in a human kidney

Hobbs, et al. "A nephron-based model of the kidneys for macro-to-micro α-particle dosimetry." Physics in Medicine & Biology 57 (2012): 4403.

Kidney S values

Table 3. Human *S*-values for the nephron model and associated values. The tables correspond to the same respective radionuclides and compartments as for table 2. The *S*-values for the kidney and cortex are included for completeness; they were calculated assuming that 100% of the alpha energy is absorbed in both cases.

^{211}At a	*S*-value (u) (Gy/Bq-s)	Absorbed energy (MeV/decay)	%	*S*-value (c) (Gy/Bq-s)
glc←glc	6.37E-05	5.85	84.57	2.06E-10
glc←prt	8.34E-06	1.16	16.77	9.40E-13
prtc←glc	3.44E-05	0.157	2.27	3.55E-12
prtc←prtc	5.27E-05	1.54	22.26	5.44E-12
prtc←prtl	5.23E-05	1.95	28.19	5.40E-12
prtc←prts	5.25E-05	1.77	25.59	5.42E-12
kid←kid	–	6.92	100	3.69E-12
cor←cor	–	6.92	100	5.60E-12

Liver anatomical model

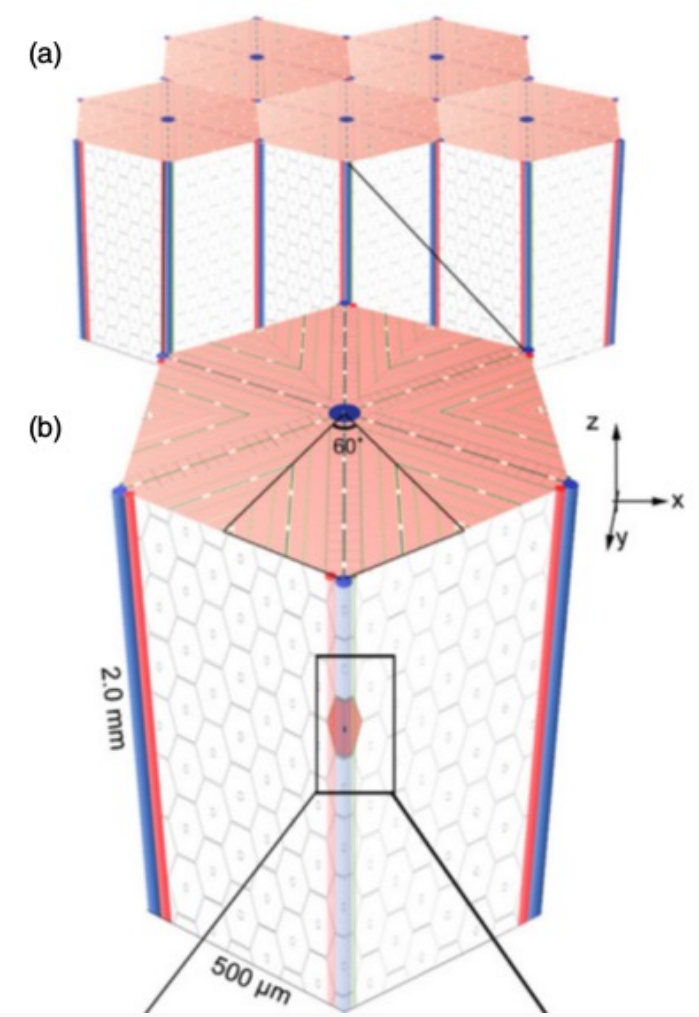

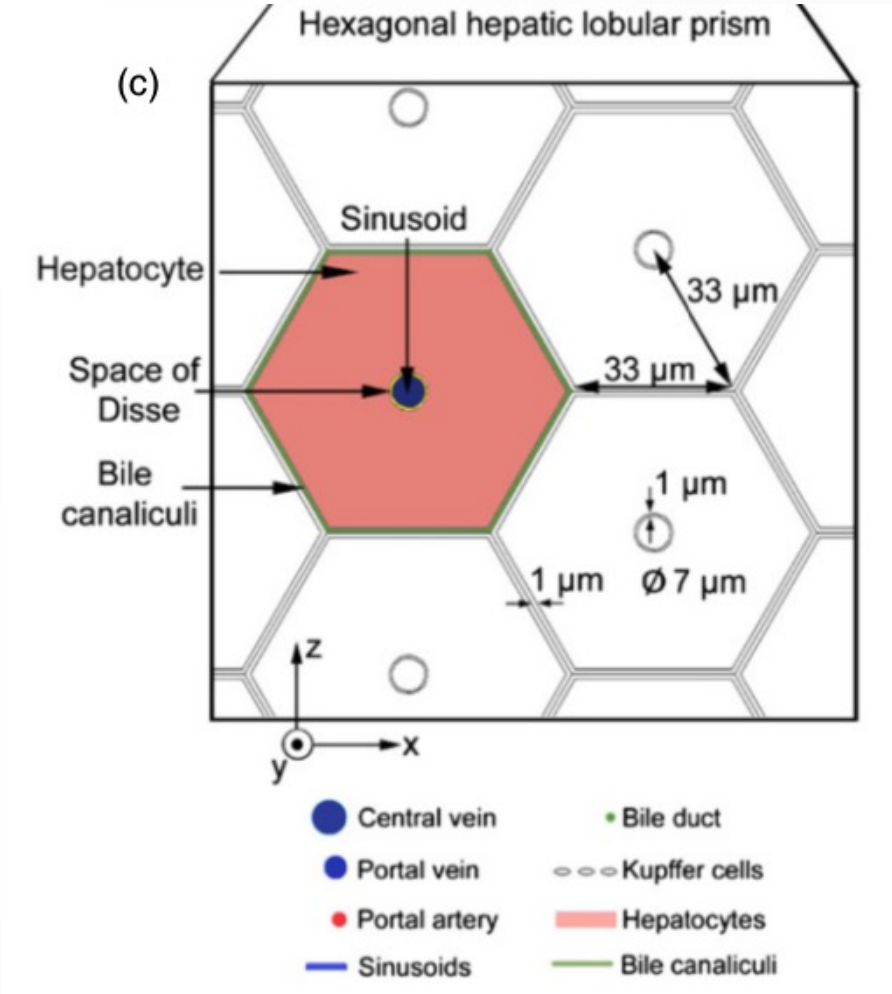

Stenvall, Anna, et al. "A small-scale anatomical dosimetry model of the liver." Physics in Medicine & Biology 59.13 (2014): 3353.

Liver S factors and absorbed doses

Source Target	(c) S values (mGy $MBq^{-1}s^{-1}$) for ^{125}I Kupffer cells[a]	Portal artery	Portal vein	Central vein	Sinusoid
Kupffer cell (central[a])	7.37E-04	4.48E-07	<1.0E-10	6.10E-08	9.30E-06
Kupffer cell(periportal[a])	7.25E-04	1.01E-06	7.80E-07	8.35E-09	8.04E-06
Hepatocyte (proximal[b]/central[c])	3.09E-06	5.70E-07	6.11E-07	5.26E-09	1.29E-06
Hepatocytes (distal[b]/periportal[c])	6.75E-07	2.11E-06	1.62E-06	2.35E-09	1.38E-06
Space of Disse (proximal[b]/central[c])	4.95E-05	5.25E-07	5.67E-07	1.67E-08	1.60E-05
Space of Disse (distal[b]/periportal[c])	7.04E-07	1.12E-06	2.06E-06	1.34E-09	1.67E-05
Portal artery	1.47E-06	4.85E-03	1.00E-04	<1.0E-10	6.36E-07
Portal vein	7.99E-07	1.02E-04	3.37E-03	<1.0E-10	7.74E-07
Central vein					
Sinusoid					

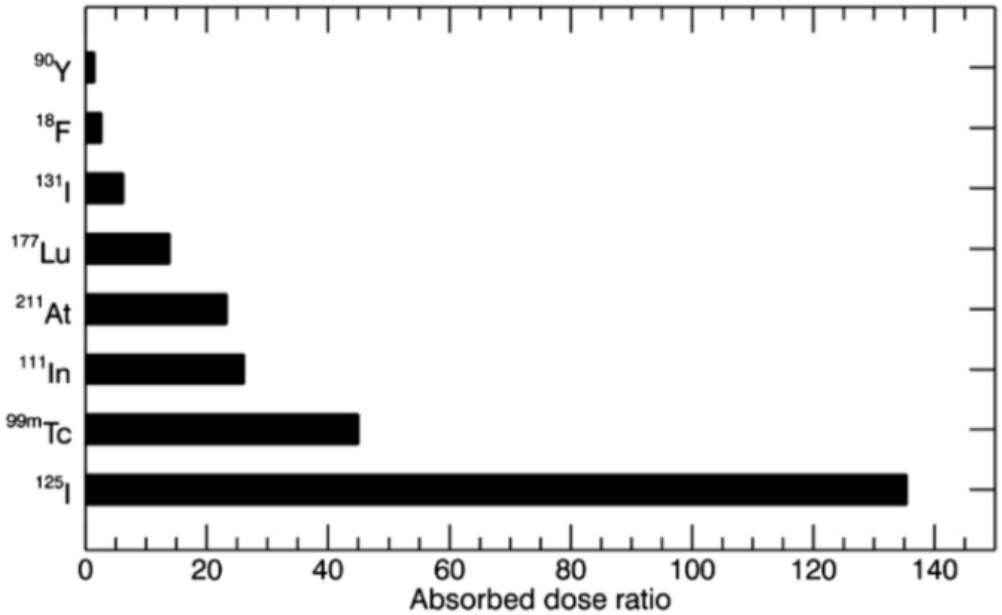

Figure 3. The ratio of the self-absorbed dose in the Kupffer cells to the average absorbed dose to the liver.

Dose heterogeneity in SIRT/TARE treatments

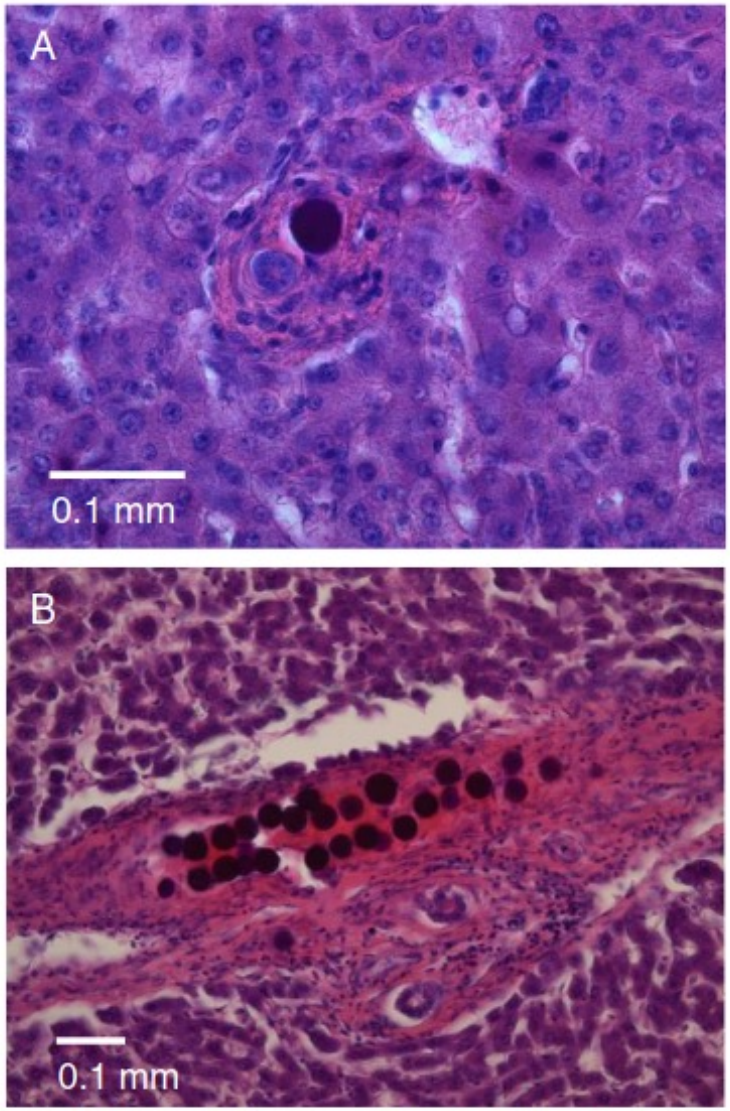

Figure 1 Light microscopy images illustrating the three main types of microsphere aggregations found in Pt 2. (A) Single isolated sphere in an arteriole in a small portal tract, magnified × 200. **(B)** A large cluster of 27 spheres in a relatively large portal tract with a wide arteriole, ×100. Based on adjacent slices, this cluster was part of a cluster of 36 spheres.

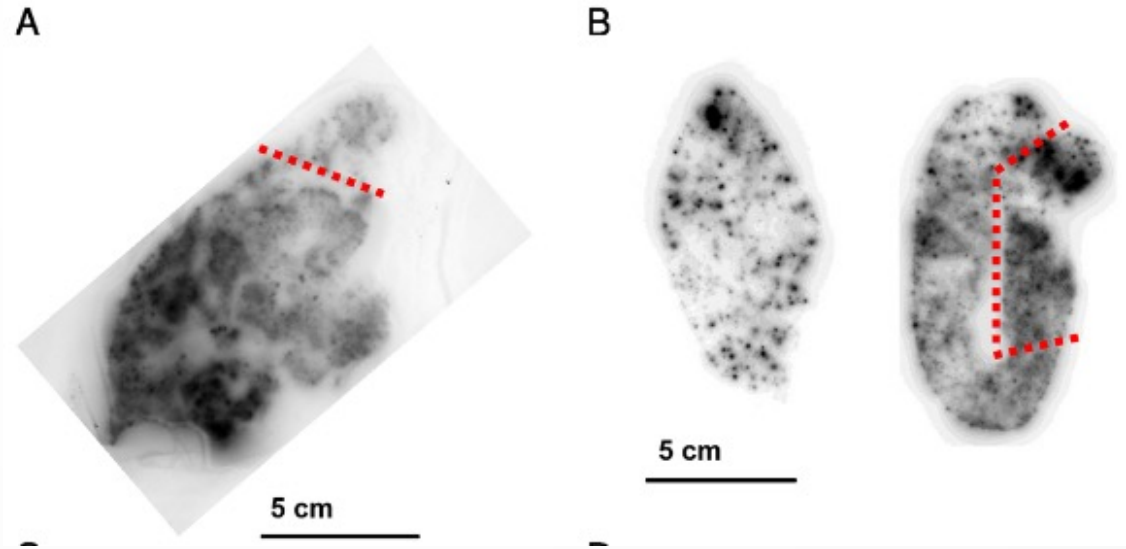

J. Högberg et al. “Heterogeneity of microsphere distribution inresected liver and tumour tissue followingselective intrahepatic radiotherapy” EJNMMI Research 2014,4:48

Bone marrow

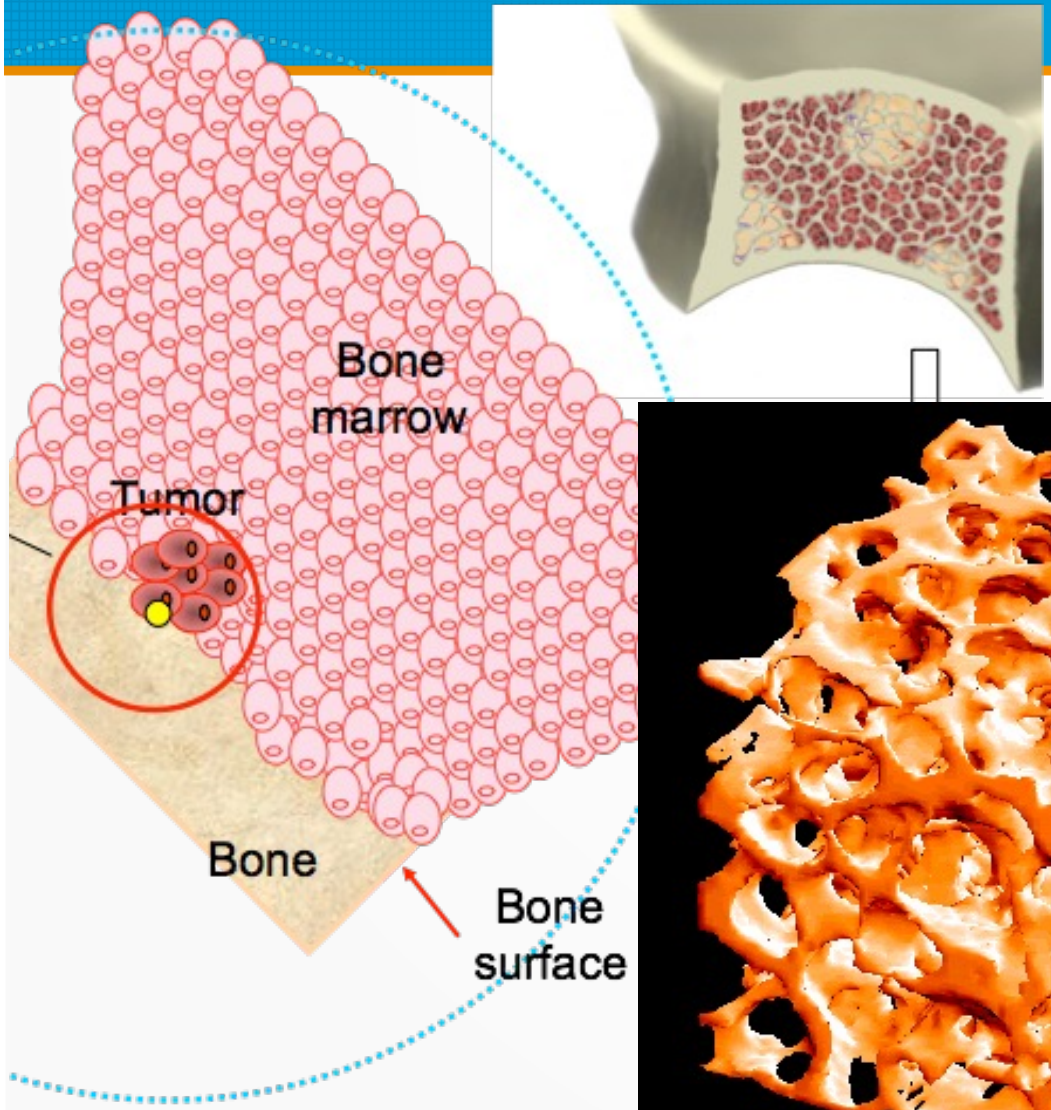

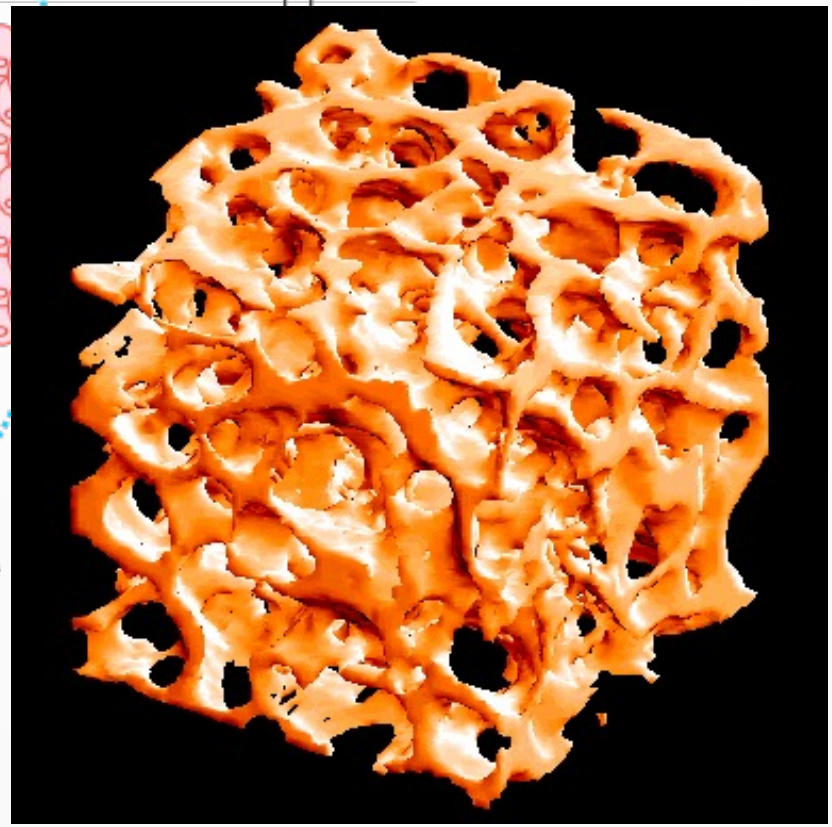

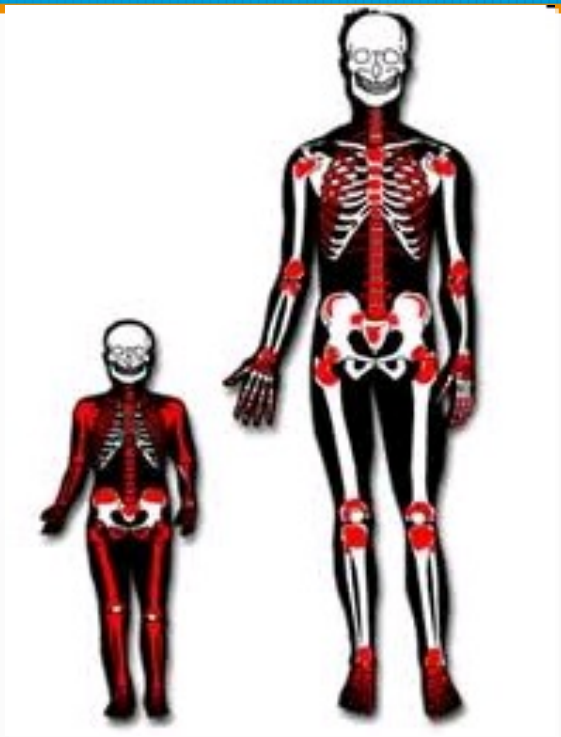

Distribution in body is sex and age dependent.
It is also modified by some disease.

Courtesy of M. Bardiès

Structure of a Long Bone

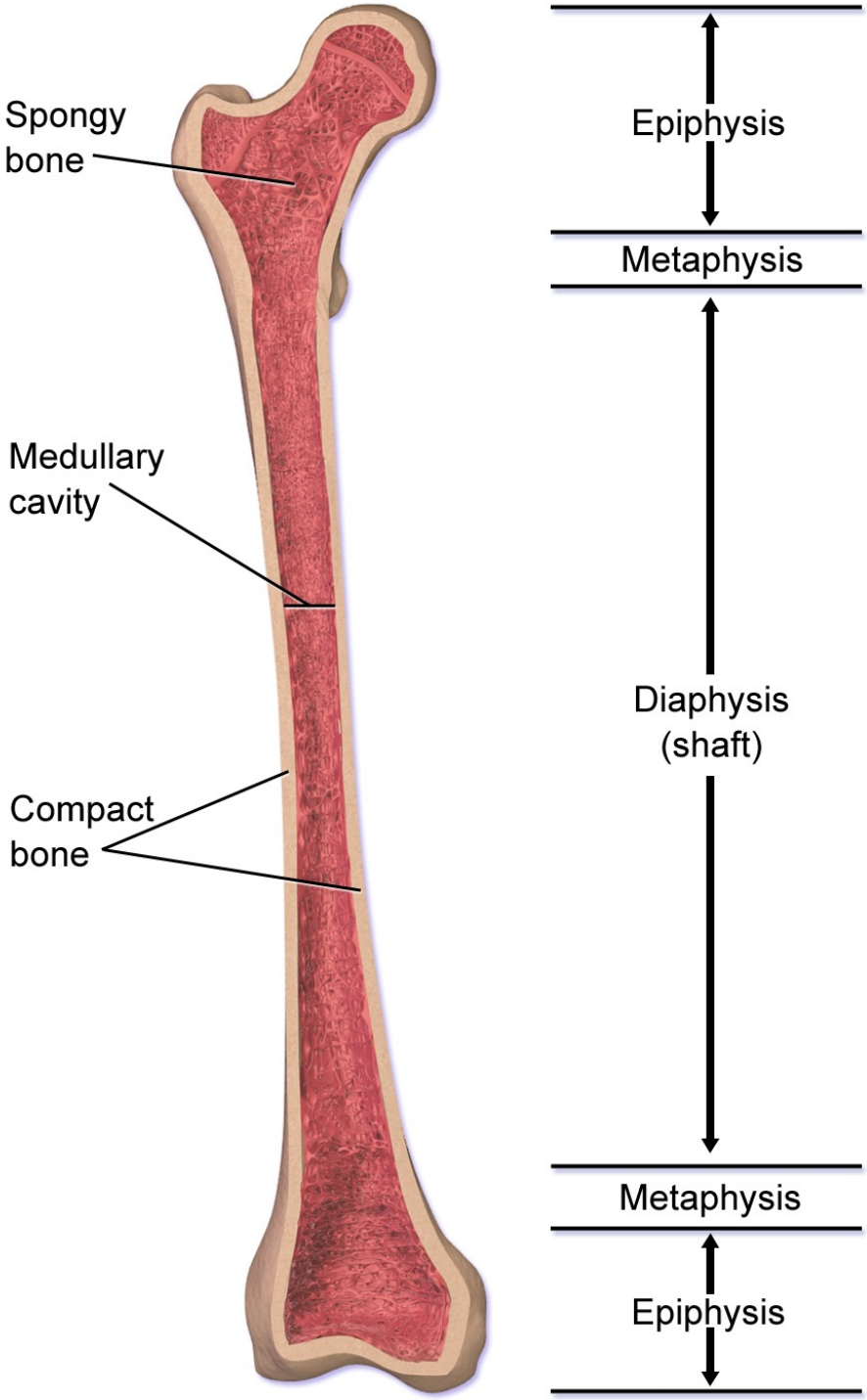

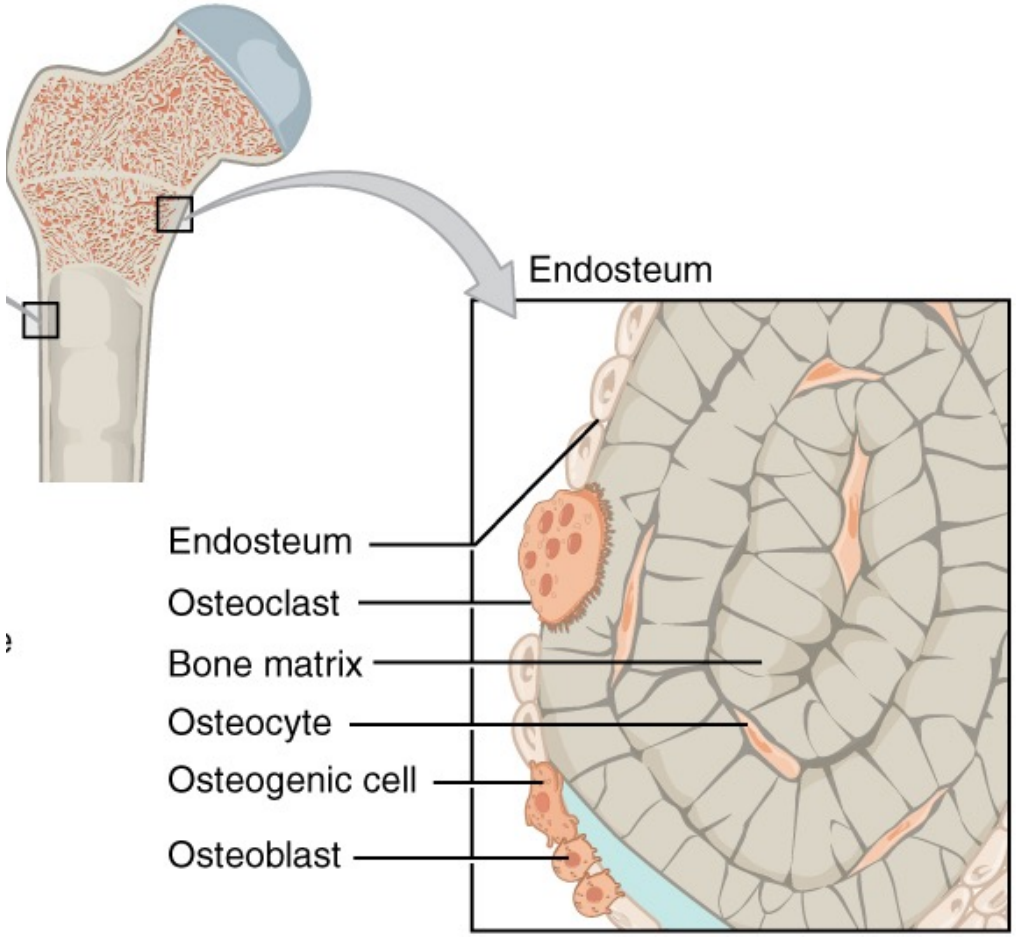

Bone marrow irradiation

Red marrow itself:

- Activity in extracellular fluid (plasma): blood
- Activity in red blood cells: blood
- Activity in bone marrow (marrow infiltrating disease)

Activity in bone (bone seeking agents):

- ^{153}Sm EDTMP, ^{166}Re HEDP, ^{223}Ra

Activity in organs and/or remainder of the body:

- Gamma component

Courtesy of M. Bardiès

Bone marrow cavity model

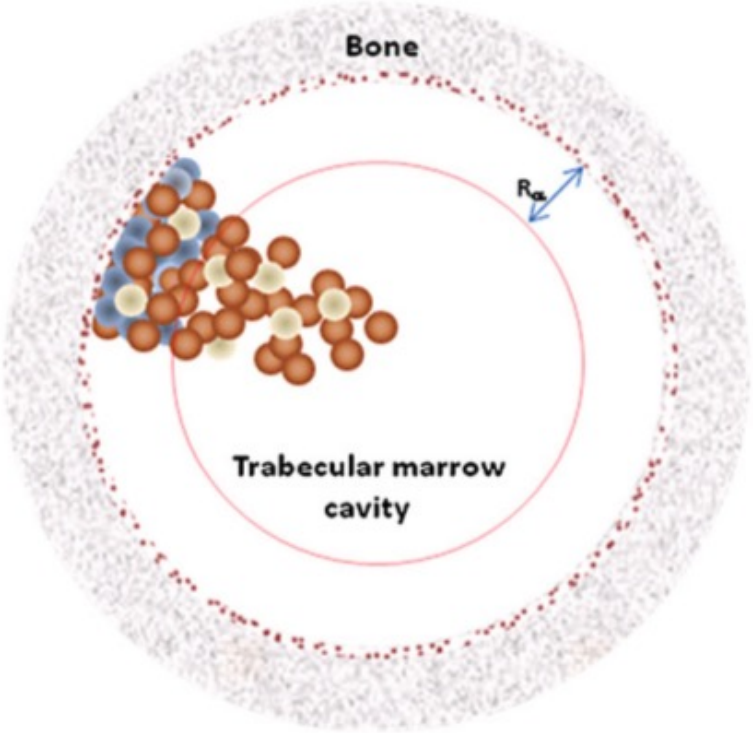

Figure 2. Representation of the marrow cavity model (not drawn to scale). The cavity is represented by a sphere of radius R_c. R_α is the range of the α-particles from ^{223}Ra decay. The blue spheres are osteoprogenitor cells, present only within shallow marrow, while the brown spheres are hematopoietic stem and progenitor cells and the white spheres are adipose cells, both present throughout the marrow cavity. The 10 μm endosteal layer is represented by the brown speckled ring.

Hobbs RF, et al. A bone marrow toxicity model for ^{223}Ra alpha-emitter radiopharmaceutical therapy. Phys Med Biol. 2012 May 21;57(10):3207

Bone marrow dynamics

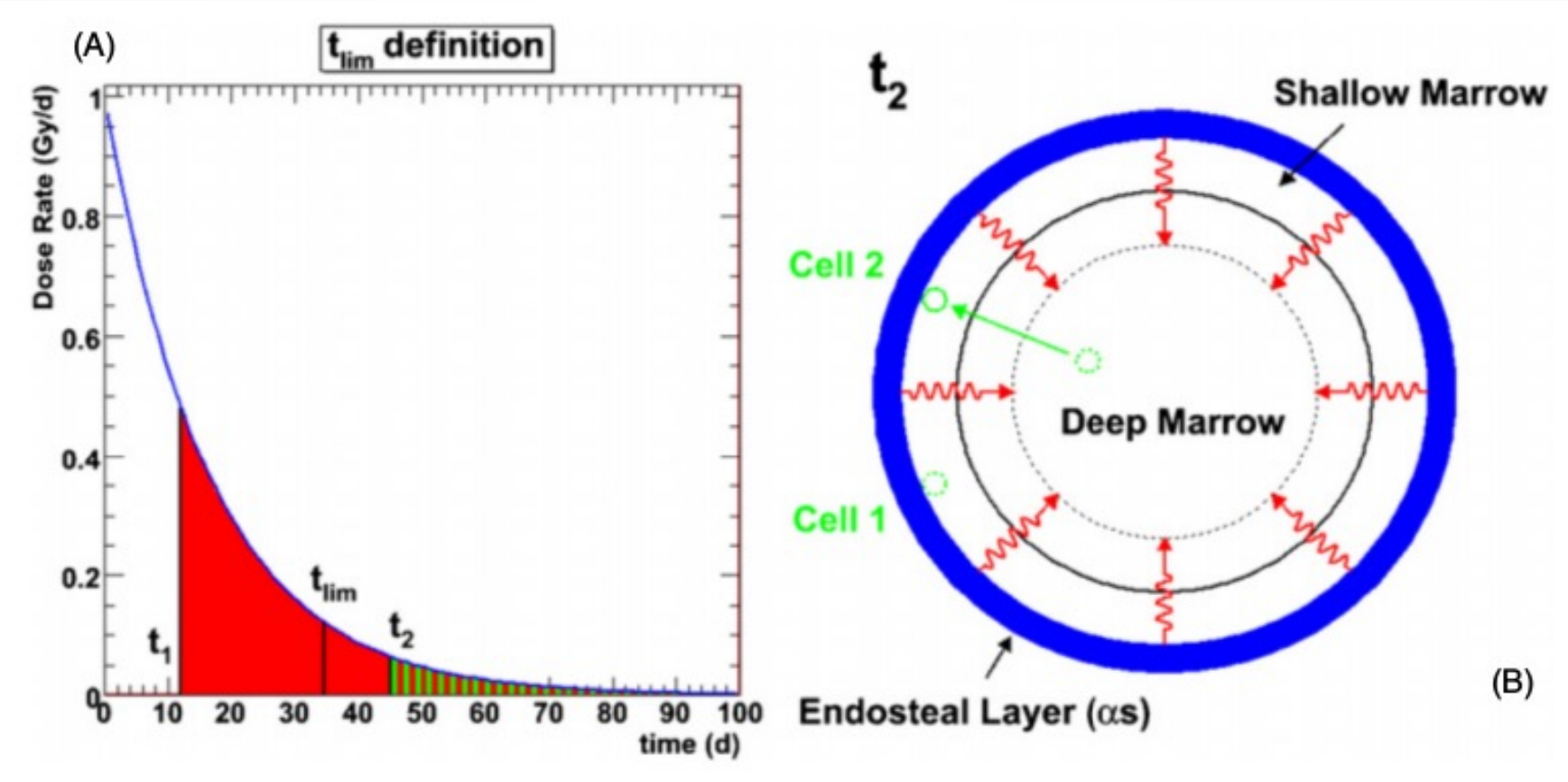

For every cellular position within the range of the α-emissions, there is a time after the start of irradiation beyond which the number of decays emanating from the trabecular surface are insufficient to deliver a reference dose (2 Gy) to a target cell occupying that position.

Bone marrow dose under a threshold

Table 2. Percentage of marrow cavity cells ('spared cell' percentages) receiving an absorbed dose below the reference value (2 Gy) as a function of marrow cavity radius, R_c, and average absorbed dose, D_{avg}, for activity localized in the endosteal layer. In this table, the average absorbed dose is calculated for the entire marrow cavity and assumes a distribution of decays as seen in the ^{223}Ra studies (endosteal layer to marrow cavity cumulated activity ratio of ~100 to 1). 'A_{EL}' indicates activity in the endosteal layer only, while '$+A_{MC}$' indicates that blood activity in the marrow cavity has been included. Both scenarios include the radial dependence of HSPC distribution.

(%)	$R_c = 500\ \mu m$		$R_c = 400\ \mu m$		$R_c = 300\ \mu m$		$R_c = 250\ \mu m$	
D_{avg} (Gy)	A_{EL}	$+A_{MC}$	A_{EL}	$+A_{MC}$	A_{EL}	$+A_{MC}$	A_{EL}	$+A_{MC}$
1	81.3	81.0	77.4	77.2	71.2	70.8	66.0	65.5
2	75.0	74.8	70.3	70.0	62.5	62.4	56.4	55.9
4	71.1	70.8	65.9	65.5	57.4	57.1	50.9	50.4
6	69.5	69.1	64.1	63.6	55.4	54.9	48.6	48.1
8	68.6	68.1	63.0	62.4	54.1	53.5	47.2	46.7
10	67.9	67.3	62.2	61.6	53.2	52.6	46.3	45.7
15	66.7	65.9	60.9	60.0	51.8	50.8	44.8	43.7
20	66.0	64.6	60.1	58.7	50.9	49.4	43.8	42.3

Multi-regional cell models

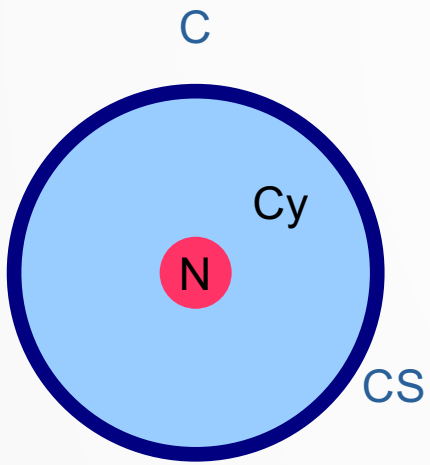

MIRD model (Goddu et al. “MIRD cellular S values” 1997)

$$D(r_k) = \sum_h \tilde{A}_h \, S(r_k \leftarrow r_h)$$

$$S(r_k \leftarrow r_h) = \sum_i \frac{\Delta_i \phi_i(r_k \leftarrow r_h)}{m_k},$$

Absorbed fractions calculated through a convolution of analytic expressions of the stopping power (Howell et al. 1989)

$$\phi_i(r_k \leftarrow r_h) = \int \Psi_{r_k \leftarrow r_h}(x) \frac{1}{E_i} \left. \frac{\mathrm{d}E}{\mathrm{d}X} \right|_{X(E_i)-x} \mathrm{d}x,$$

Range straggling and non-local energy deposition by energetic secondary particles are neglected

Significance of the MC calculation

Table 2. *S*-factors for monoenergetic electrons in cellular spheres with $R_C = 10\ \mu m$ and $R_N = 5\ \mu m$.

Electron energy (keV)	*S*(C←C) (Gy/Bq s)		*S*(C←CS) (Gy/Bq s)		*S*(N←N) (Gy/Bq s)		*S*(N←Cy) (Gy/Bq s)		*S*(N←CS) (Gy/Bq s)	
	MIRD	MC	MIRD	MC	MIRD	MC	MIRD	MC	MIRD	MC
1	3.82E−05	3.81E−05 (−0.26)	1.91E−05	1.90E−05 (−0.52)	3.04E−04	3.05E−04 (+0.33)	2.55E−07	1.45E−07 (−43.14)	0.00E+00	0.00E+00 (0.00)
10	3.35E−04	3.48E−04 (+3.88)	1.76E−04	1.80E−04 (+2.27)	2.30E−03	2.51E−03 (+9.13)	1.10E−04	7.87E−05 (−28.45)	0.00E+00	0.00E+00 (0.00)
20	4.52E−03	6.32E−03 (+39.82)	3.11E−03	4.66E−03 (+49.84)	3.81E−02	4.04E−02 (+6.04)	4.61E−03	6.59E−03 (+42.95)	2.23E−03	4.03E−03 (+80.72)
30	3.18E−03	3.52E−03 (+10.69)	2.15E−03	2.48E−03 (+15.34)	2.78E−02	2.72E−02 (−2.16)	3.23E−03	3.66E−03 (+13.31)	1.50E−03	1.86E−03 (+24.00)
50	2.14E−03	2.10E−03 (−1.87)	1.43E−03	1.43E−03 (0)	1.90E−02	1.76E−02 (−7.37)	2.17E−03	2.23E−03 (+2.76)	9.90E−04	1.03E−03 (+4.04)
70	1.68E−03	1.59E−03 (−5.36)	1.12E−03	1.08E−03 (−3.57)	1.50E−02	1.35E−02 (−10.00)	1.70E−03	1.64E−03 (−3.53)	7.71E−04	7.84E−04 (+1.69)
100	1.31E−03	1.22E−03 (−6.87)	8.79E−04	8.18E−04 (−6.94)	1.18E−02	1.04E−02 (−11.86)	1.33E−03	1.28E−03 (−3.76)	6.03E−04	5.92E−04 (−1.82)
300	7.22E−04	6.46E−04 (−10.53)	4.82E−04	4.31E−04 (−10.58)	6.50E−03	5.38E−03 (−17.23)	7.30E−04	7.39E−04 (+1.23)	3.30E−04	3.30E−04 (0)
500	6.10E−04	5.46E−04 (−10.49)	4.07E−04	3.59E−04 (−11.79)	5.49E−03	4.37E−03 (−20.40)	6.18E−04	6.42E−04 (+3.88)	2.79E−04	3.00E−04 (+7.53)
700	5.71E−04	5.06E−04 (−11.38)	3.81E−04	3.33E−04 (−12.60)	5.14E−03	4.06E−03 (−21.01)	5.78E−04	6.23E−04 (+2.60)	2.61E−04	2.78E−04 (+6.51)
1000	5.51E−04	4.79E−04 (−13.07)	3.68E−04	3.17E−04 (−13.86)	4.96E−03	3.84E−03 (−22.58)	5.57E−04	5.64E−04 (+1.24)	2.52E−04	2.72E−04 (+7.94)

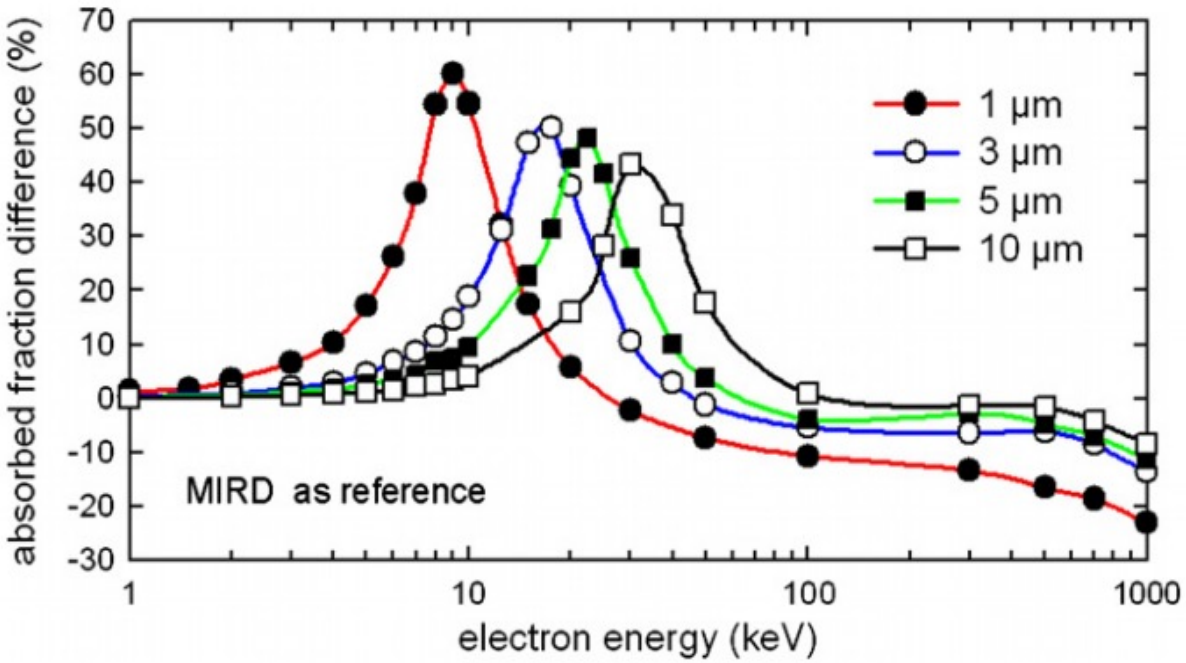

Bousis et al. "A Monte Carlo study of cellular S-factors for 1 keV to 1 MeV electrons" *Phys. Med. Biol.* 2009, **54** 5023

Anti-angiogenic effects of RF

In solid tumors with rapidly-growing neo-vascularization, the combination between cytotoxic and anti-angiogenic effects is desirable.

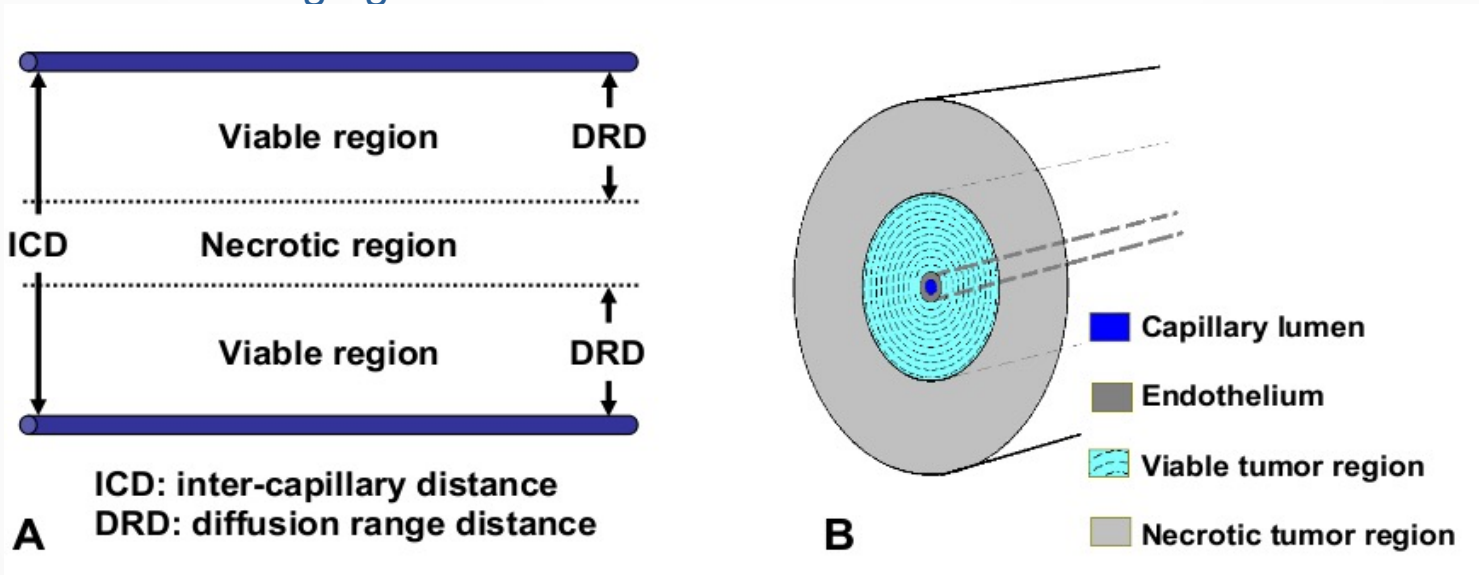

MC EGS

X. Zhu,...A. Kassis "Solid-Tumor Radionuclide Therapy Dosimetry: New Paradigms in View of Tumor Microenvironment and Angiogenesis" Med. Phys. 2010

Maximum dose to the capillary endotelium:

- Low diffusion range of the RF
- Low range of the radiations (Auger, α)

Maximum dose to the viable tumor:

- Low diffusion range of the RF
- High range of the radiations (β)

  OR
- High diffusion range of the RF

Anti-angiogenic effects of RF:
Extension to clinical radionuclides

E. Amato, et al. "A Monte Carlo approach to small-scale dosimetry of solid tumour microvasculature for nuclear medicine therapies with ^{223}Ra-, ^{131}I-, ^{177}Lu- and ^{111}In-labelled radiopharmaceuticals." Physica Medica 31 (2015): 536

Model of tumour capillary vessel surrounded by target tissue.

- ^{223}Ra (^{219}Rn, ^{215}Po, ^{211}Pb, ^{211}Bi, ^{211}Po, ^{207}Tl)
- ^{131}I
- ^{177}Lu
- ^{111}In

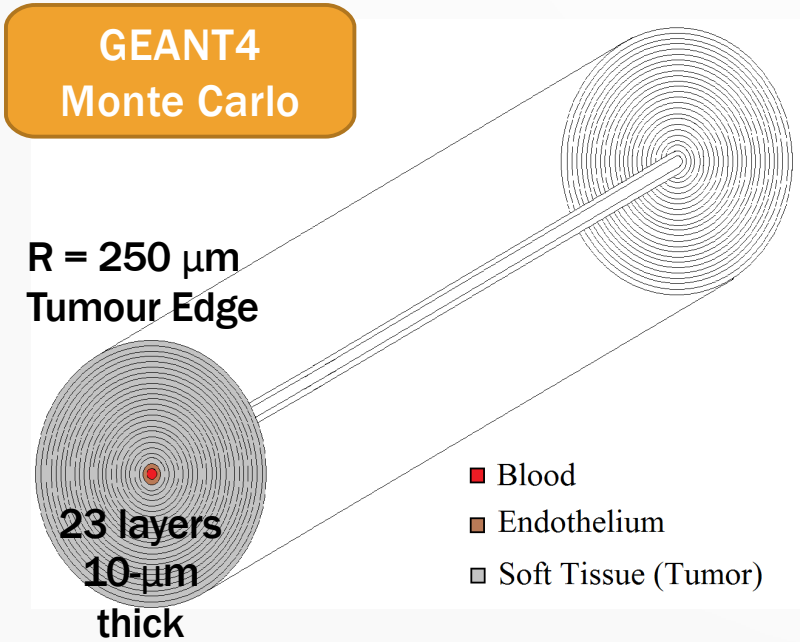

Radial distribution configurations of the radionuclides used.

Configuration#	Regions	Range (μm)
A	Blood	0–10
B	Endothelial cells	10–20
C	Blood + E.C.	0–20
D	E.C. + Tumour	10–50
E	E.C. + Tumour	10–100
F	E.C. + Tumour	10–150
G	E.C. + Tumour	10–200

RESULTS – SOURCE IN BLOOD

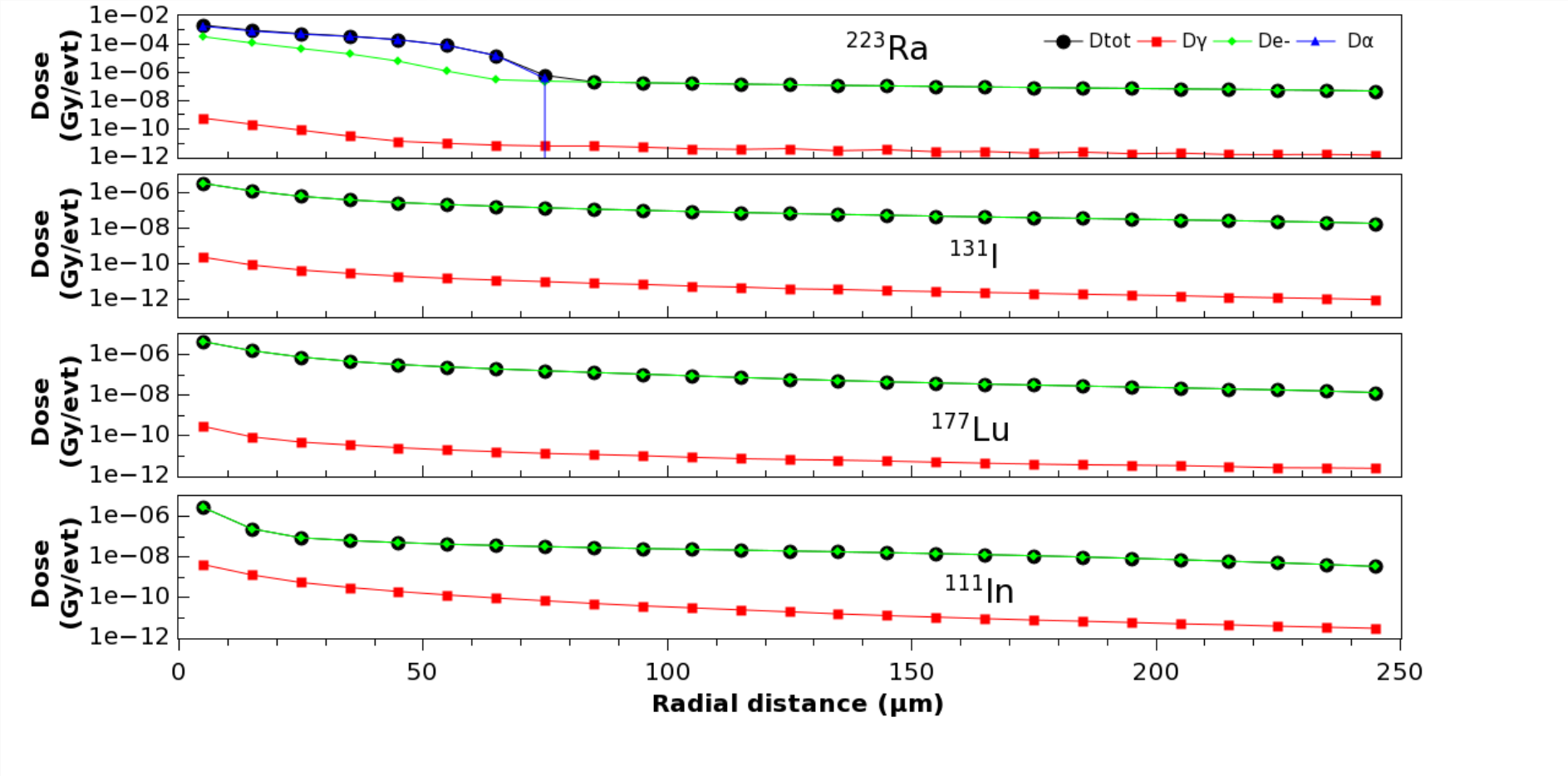

Radial dose profiles for sources located in blood (configuration A).

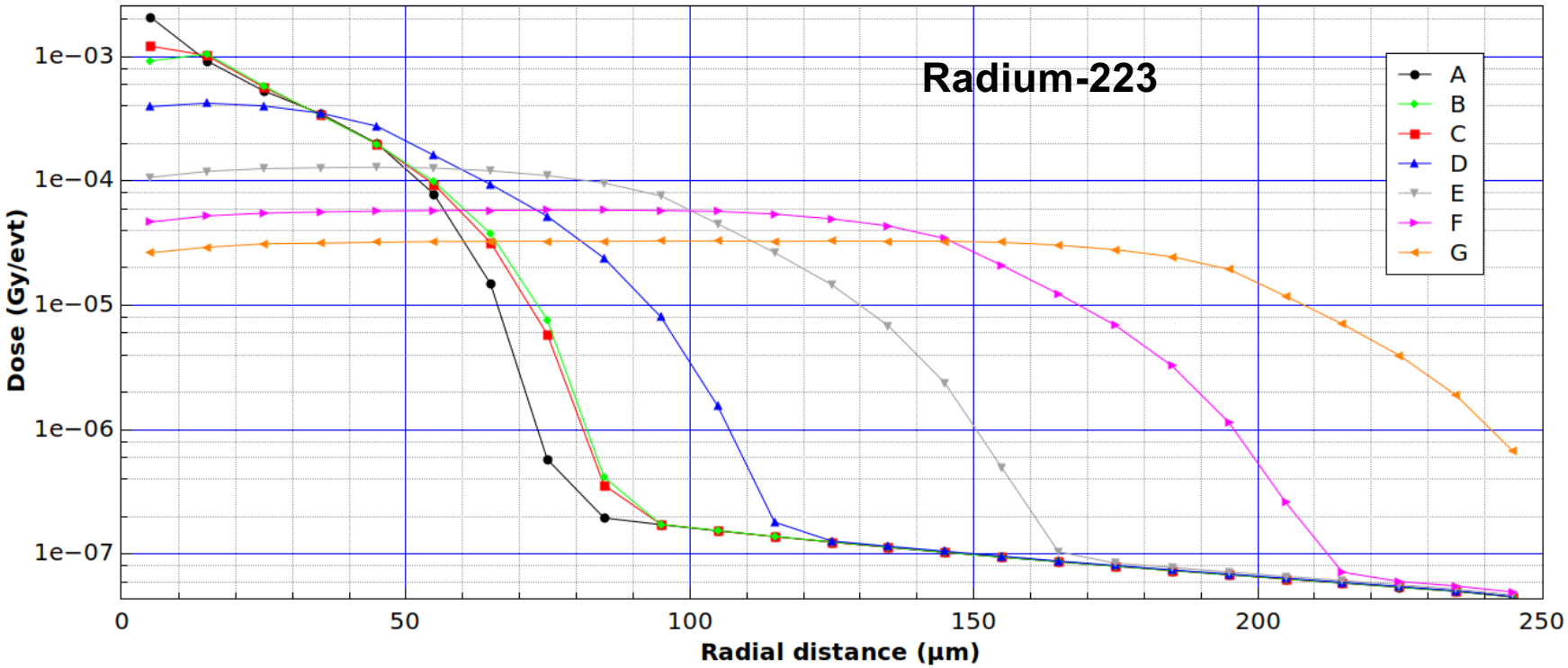
Radium-223
A
B
C
D
E
F
G
Dose (Gy/evt)
1e−03
1e−04
1e−05
1e−06
1e−07
0
50
100
150
200
250
Radial distance (µm)

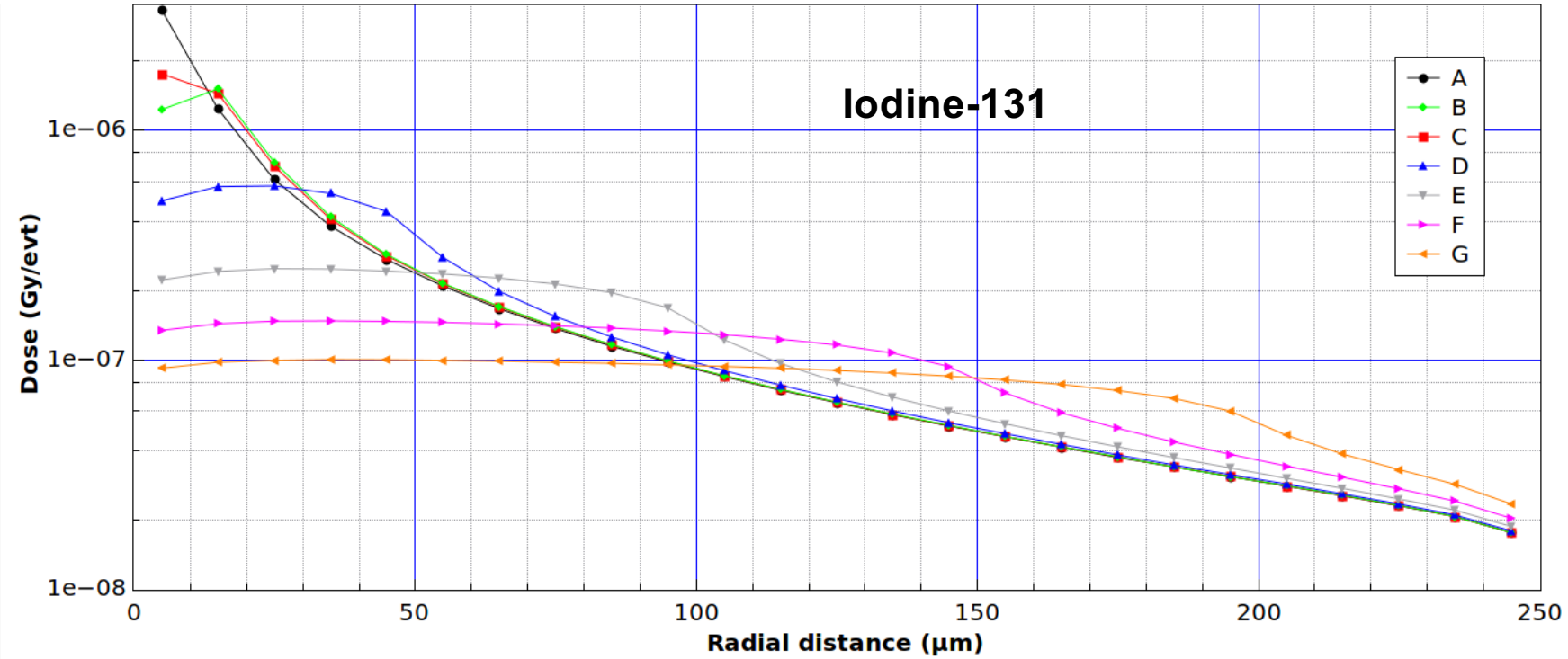
Iodine-131
A
B
C
D
E
F
G
Dose (Gy/evt)
1e−06
1e−07
1e−08
0
50
100
150
200
250
Radial distance (µm)

Endothelial Cell Mean Dose (ECMD) and Tumour Edge Mean Dose (TEMD)